Report No. 5495

DETECTION THRESHOLDS FOR TRACKING IN CLUTTER - A CONNECTION BETWEEN ESTIMATION AND SIGNAL PROCESSING

Thomas E. Fortmann, Yaakov Bar-Shalom,
Molly Scheffé, and Saul Gelfand

7 December 1983

Prepared by:

Bolt Beranek and Newman Inc.
10 Moulton Street
Cambridge, Massachusetts 02238

Prepared for:

Naval Analysis Program
Office of Naval Research
800 North Quincy Street
Arlington, Virginia 22217

Attention: 411SP

DEFENSE TECHNICAL INFORMATION CENTER

Information for the Defense Community

DTIC® has determined on Month 04 Day 27 Year 2008 *that this Technical Document has the Distribution Statement checked below. The current distribution for this document can be found in the DTIC® Technical Report Database.*

☒ **DISTRIBUTION STATEMENT A.** Approved for public release; distribution is unlimited.

☐ **© COPYRIGHTED.** U.S. Government or Federal Rights License. All other rights and uses except those permitted by copyright law are reserved by the copyright owner.

☐ **DISTRIBUTION STATEMENT B.** Distribution authorized to U.S. Government agencies only. Other requests for this document shall be referred to controlling office.

☐ **DISTRIBUTION STATEMENT C.** Distribution authorized to U.S. Government Agencies and their contractors. Other requests for this document shall be referred to controlling office.

☐ **DISTRIBUTION STATEMENT D.** Distribution authorized to the Department of Defense and U.S. DoD contractors only. Other requests shall be referred to controlling office.

☐ **DISTRIBUTION STATEMENT E.** Distribution authorized to DoD Components only. Other requests shall be referred to controlling office.

☐ **DISTRIBUTION STATEMENT F.** Further dissemination only as directed by controlling office or higher DoD authority.

Distribution Statement F is also used when a document does not contain a distribution statement and no distribution statement can be determined.

☐ **DISTRIBUTION STATEMENT X.** Distribution authorized to U.S. Government Agencies and private individuals or enterprises eligible to obtain export-controlled technical data in accordance with DoDD 5230.25.

TABLE OF CONTENTS

ABSTRACT

Tracking performance depends upon the quality of the measurement data. In the Kalman-Bucy filter and other trackers, this dependence is well-understood in terms of the measurement noise covariance matrix, which specifies the uncertainty in the values of the measurement inputs. The measurement noise and process noise covariances determine via the Riccati equation, the state estimation error covariance. When the origin of the measurements is also uncertain, one has the widely-studied problem of data association (or data correlation), and tracking performance depends critically on additional parameters, primarily the probabilities of detection and false alarm. In this paper we derive a modified Riccati equation that quantifies (approximately) the dependence of the state error covariance on these parameters. We also show how to use a ROC curve in conjunction with the above relationship to determine an optimal detection threshold in the signal processing system that provides measurements to the tracker. A validation of the modified Riccati equation is also presented.

1. INTRODUCTION

Garden-variety tracking problems involve processing measurements (e.g., range and azimuth observed by a sensor) from a target of interest and producing, at each time step, an estimate of the target's current position and velocity vectors. Uncertainties in the target motion and in the measured values, usually characterized as random noise, lead to corresponding uncertainties in the target state.

A common and versatile approach to such problems involves assuming that the state dynamics and the measurements are both corrupted by additive, white, possibly Gaussian noise; the solution is then the celebrated Kalman-Bucy filter [1-5], which is the conditional mean state estimator, best linear estimator, maximum a posteriori estimator, maximum likelihood estimator, or least-squares estimator, depending upon one's point of view. The parameters that determine tracking performance in such a filter are the system matrices in the equations describing target state dynamics and measurements, which will be considered fixed for the purposes of this discussion, and the covariance matrices of the process and measurement noises, which specify the uncertainties in target motion and measured values, respectively.

In many tracking problems, particularly those arising in surveillance, there is additional uncertainty regarding the origin of the received data, which may (or may not) include measurements from the target(s) of interest, interfering targets, or random clutter (false alarms). This leads to the problem of data association or data correlation, which has been attacked on a number of fronts [6-14] and surveyed in [15-17]. In this situation, tracking performance depends not only upon the noise

covariances, but also upon the amount of uncertainty in measurement origin. In some of the approaches cited above [6-10], this dependence is explicit and is characterized in terms of the detection probability P_D and false alarm probability P_F (which is proportional to clutter density).

In typical applications, measurement data are provided to a tracker by upstream signal processing and detection algorithms, as indicated in Figure 1. The process noise covariances are normally selected on the basis of experience and intuition (i.e., they are guessed). The measurement noise covariances are either provided by the signal processing algorithm, as shown in the figure, or they are selected in the same manner as the process noise. In any case, the true noise levels are usually fixed by target dynamics and sensor configuration and cannot be adjusted on line.

Detection and false alarm probabilities, on the other hand, are highly interdependent and adjustable via a detection threshold: raising the threshold lowers both probabilities, and vice-versa. This relationship, which also depends parametrically on the signal-to-noise ratio (SNR), is usually characterized by means of a set of receiver operating characteristic (ROC) curves, as discussed below in Section 4. The threshold is typically set by choosing a design point on the applicable ROC curve, based on the perceived tradeoffs between false alarms and missed detections. However, to the best of our knowledge, these tradeoffs have never included any systematic or quantitative consideration of the effects downstream on data association and tracking performance.

In this paper we shall describe such a quantitative

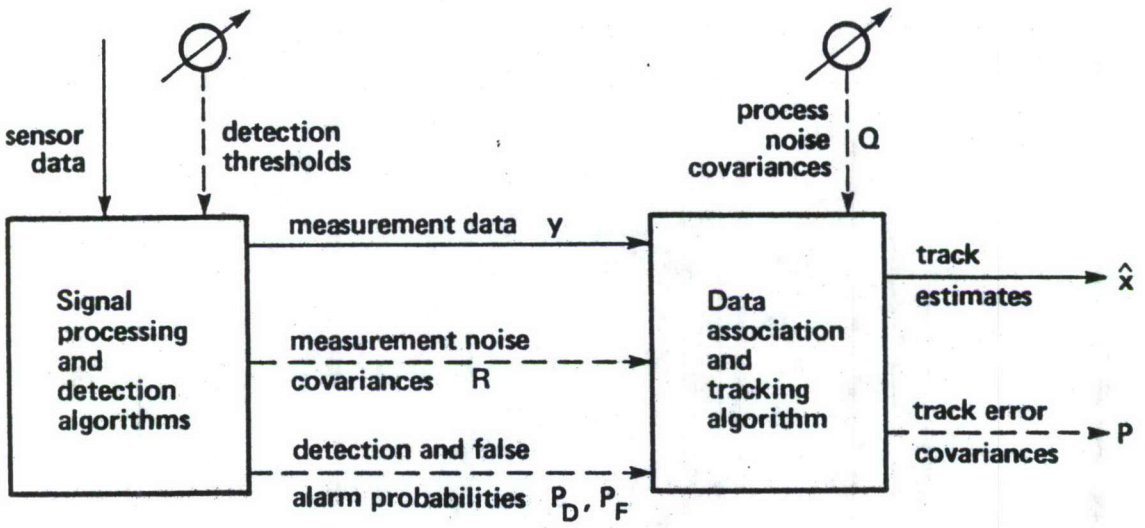

FIG. 1. TRACKING SYSTEM BLOCK DIAGRAM

relationship. The dependence of a tracker's error covariance upon the detection and false alarm probabilities is explicitly (but approximately) characterized by a scalar parameter q_2 in the covariance equation, called the modified Riccati equation. This scalar parameter depends upon the probabilities of detection and false alarm, and also upon the volume of the data association gate, which in turn depends on the state error covariance matrix $\underline{P}$. The modified Riccati equation can be iterated to convergence, yielding a steady-state $\bar{\underline{P}}$, and tracking performance can be characterized by a scalar metric such as determinant ($\bar{\underline{P}}$), trace ($\bar{\underline{P}}$), or (in surveillance applications) root-mean-square position error. This result is important for the following reasons:

1. Contour plots of the scalar tracking performance metric as a function of detection probability and false alarm

probability form a set of tracker operating characteristic (TOC) curves, which can be superimposed on ROC curves for the detector or receiver of interest in order to determine graphically the operating points that optimize tracker performance.

2. The stability of the tracking process depends critically on the detection and false alarm probabilities; indeed, a region of apparent instability of the modified Riccati equation exists in the P_D-P_F plane of the TOC curves. The implication of this for detector/receiver design is that there are settings of the detection parameters that render the output useless for downstream tracking.

3. Allocation of tracking resources (both computation and communication) requires prediction of future state error covariances under various resource configurations, i.e., as a function of detection and false alarm probability and of process and measurement noise covariance.

4. The same derivations provide a solution to the related problem of determining the statistical properties of the modified likelihood function [18], used for decision making (e.g. maneuver detection) when measurement origins are uncertain.

In Section 2 the problem of relating tracking performance to detection and false alarm probabilities is formulated in the context of probabilistic data association. The key TOC results are derived in Section 3, followed by examples in Section 4. Conclusions and suggestions for further research are found in Section 5. Discussion of the numerical operations, derivation of complex mathematical expressions, and a description of the simulations used to validate the modified Riccati equation may be found in Appendices A-E.

2. PROBLEM FORMULATION

Consider a dynamic system (target model) of the usual form,

$$\underline{x}_{k+1} = \underline{F}\underline{x}_k + \underline{G}\underline{w}_k \tag{1}$$

$$\underline{y}_k = \underline{H}\underline{x}_k + \underline{v}_k \tag{2}$$

where $\underline{x}$ is the state vector, $\underline{y}$ is the measurement vector, $\underline{w}$ and $\underline{v}$ are zero-mean, mutually independent, white, gaussian noise vectors with covariance matrices $\underline{Q}$ and $\underline{R}$, respectively, and k is a discrete time index. The matrices $\underline{F}$, $\underline{G}$, $\underline{H}$, $\underline{Q}$, and $\underline{R}$ are assumed known and their dependence on k is suppressed here for notational convenience. The initial state is assumed gaussian with mean $\hat{\underline{x}}_{\emptyset|\emptyset}$ and covariance $\underline{P}_{\emptyset|\emptyset}$. A typical state vector would include position and velocity variables, as well as other information that relates to the specific type of platform being tracked, and typical dynamics would assume straight-line or great-circle target motion with disturbances from the process noise $\underline{w}$.

The tracker's estimate of the target state $\underline{x}_k$ at time k, given data up to time i, is denoted $\hat{\underline{x}}_{k|i}$. The error in this estimate is $\tilde{\underline{x}}_{k|i} = \underline{x}_k - \hat{\underline{x}}_{k|i}$, with error covariance matrix $\underline{P}_{k|i} = E\{\tilde{\underline{x}}_{k|i}\tilde{\underline{x}}'_{k|i}\}$, where E denotes expectation. The discrete-time Kalman-Bucy filter [2-5] propagates these in two stages. The prediction stage accounts for time evolution,

$$\hat{\underline{x}}_{k|k-1} = \underline{F}\hat{\underline{x}}_{k-1|k-1} \tag{3}$$

$$\underline{P}_{k|k-1} = \underline{F}\underline{P}_{k-1|k-1}\underline{F}' + \underline{G}\underline{Q}\underline{G}' \tag{4}$$

starting from the initial conditions $\hat{\underline{x}}_{\emptyset|\emptyset}$ and $\underline{P}_{\emptyset|\emptyset}$. The update stage compares the incoming measurement $\underline{y}_k$ with the predicted measurement $\hat{\underline{y}}_{k|k-1} = \underline{H}\hat{\underline{x}}_{k|k-1}$ to form the *innovation* vector

$$\tilde{\underline{y}}_k \triangleq \underline{y}_k - \hat{\underline{y}}_{k|k-1} \tag{5}$$

whose covariance matrix is

$$\underline{S}_k \triangleq E\{\tilde{\underline{y}}_k\tilde{\underline{y}}_k'\} = \underline{H}\underline{P}_{k|k-1}\underline{H}' + \underline{R} \tag{6}$$

The state and covariance are then updated via

$$\hat{\underline{x}}_{k|k} = \hat{\underline{x}}_{k|k-1} + \underline{W}_k\tilde{\underline{y}}_k \tag{7}$$

$$\begin{aligned}\underline{P}_{k|k} &= (\underline{I}-\underline{W}_k\underline{H})\underline{P}_{k|k-1}(\underline{I}-\underline{W}_k\underline{H})' + \underline{W}_k\underline{R}\underline{W}_k' \\ &= \underline{P}_{k|k-1} - \underline{W}_k\underline{S}_k\underline{W}_k'\end{aligned} \tag{8}$$

where

$$\underline{W}_k \triangleq \underline{P}_{k|k-1}\underline{H}'\underline{S}_k^{-1} \tag{9}$$

is the filter gain matrix. The resulting state estimate, under

the above assumptions, is the conditional mean $\hat{\underline{x}}_{k|k} = E\{\underline{x}_k | Y^k\}$ where Y^k denotes all data vectors $\underline{y}_i$ for $i \leq k$.

Equations (4) and (8) comprise the matrix Riccati equation [1-5] for the state estimation covariance that characterizes the tracker's performance. This iterative equation is deterministic, since for a linear filter, the estimation accuracy is independent of the data.

In order to avoid clouding the discussion to follow, this brief summary ignores a number of complications that arise in practice. If the system is nonlinear, for example, then it can usually be linearized and the same basic equations can be applied to deviations from the nominal trajectory [3, 5]. If the target occasionally deviates from the assumed motion model, e.g., by maneuvering, then some decision-making or other machinery must be provided to deal with these instances.

In multi-sensor problems, the size and composition of the measurement vector often varies from one time to the next; in other words, $\underline{y}_k$ is composed of independent subvectors from various sensors, any subset of which may be present at a given time. Moreover, in the problem of interest here, each sensor supplies not one but several subvectors that must be associated with targets. We will avoid the resulting notational morass by restricting equations (5)-(8) to apply to a measurement subvector $\underline{y}_k$ from a single sensor. In addition, we will suppress the time index k from all variables except $\underline{P}, \underline{W}, \underline{S}$, and Y, except where it is required for clarity. Without any loss of generality, the data association problem may now be formulated as follows.

At each time step, the sensor provides a set of candidate measurements to be associated with targets (or rejected). In

most approaches, some preselection is done by forming a validation gate around the predicted measurement from each target and selecting those detections that lie within the gate. There are many different approaches to establishing a correspondence between candidate measurements and targets, some of which were cited above in Section 1.

In this paper we shall focus on the probabilistic data association (PDA) method [6-8,15], although the results are relevant to other methods [9, 10] in which similar machinery is used. The candidate measurements in a gate at time k are denoted $\underline{y}_j$, j=1,...m, and their corresponding innovations are

$$\underline{\tilde{y}}_j \triangleq \underline{y}_j - \underline{\hat{y}}, \qquad j=1,...m \tag{10}$$

The term measurement will be used interchangeably for $\underline{y}_j$ and $\underline{\tilde{y}}_j$, since they contain equivalent information [5].

Considering a single target independently of any others, χ_j denotes the event that the j-th measurement belongs to that target and $\chi_\emptyset$ the event that none of the measurements belongs to it (no detection). The PDA approach builds upon the assumptions that the estimation errors $\underline{\tilde{x}}$ and $\underline{\tilde{y}}$ have gaussian densities at each time step (this is approximate, since there is an exponentially growing tree of possible measurement sequence hypotheses and the true densities are gaussian mixtures-- weighted sums of gaussians). It is also assumed that the correct measurement is detected with probability P_D (independently at each time) and that all other measurements are Poisson-distributed with parameter CV, where V is the volume of the validation gate and C is the expected number of false

measurements per unit volume.[1] with Note that $C = P_F/V_c$, where V_c is the volume of one resolution cell (see Section 4) and P_F is the probability of false alarm in each cell.

The gate is normally a g-sigma ellipsoid $\{\underline{\nu} : \underline{\nu}'\underline{S}_k^{-1}\underline{\nu} \leq g^2\}$ and P_G is the probability that the correct measurement, if detected, lies within the gate.[2] The gate volume is thus

$$V = c_M g^M |\underline{S}_k|^{1/2} \tag{11}$$

where M is the dimension of $\underline{\nu}$ and $c_M = \pi^{M/2}/\Gamma(M/2+1)$ is the volume of the M-dimensional unit sphere ($c_1=2$, $c_2=\pi$, $c_3=4\pi/3$, etc.).

The conditional mean estimate $\hat{\underline{x}}$ is obtained from (7) by using the combined (weighted) innovation

$$\underline{\nu} \triangleq \sum_{j=1}^{m} \beta_j \underline{\nu}_j \tag{12}$$

where $\beta_j \triangleq P\{\theta_j | Y^k\}$, $j=\emptyset,1,\ldots m$, is the posterior probability that the j-th measurement (or no measurement, for $j=\emptyset$) is the correct one. These probabilities are given by the following expressions (see Appendix C):

---

[1] Equivalently, the number n of false measurements has probability mass function $p(n) = e^{-CV}(CV)^n/n!$ and the location of each false measurement is uniformly distributed in the gate.

[2] This is just the gaussian probability mass in the gate, which is often assumed to be unity in practice, since $P_G > .99$ whenever $g > M^{1/2}+2$.

$$\beta_j = \frac{\exp(-\underline{\nu}_j' \underline{S}_k^{-1} \underline{\nu}_j / 2)}{b + \sum_{i=1}^{m} \exp(-\underline{\nu}_i' \underline{S}_k^{-1} \underline{\nu}_i / 2)}, \quad j=1,\ldots m \tag{13}$$

$$\beta_\emptyset = \frac{b}{b + \sum_{i=1}^{m} \exp(-\underline{\nu}_i' \underline{S}_k^{-1} \underline{\nu}_i / 2)} \tag{14}$$

where

$$\begin{aligned} b &\triangleq (2\pi)^{M/2} C |\underline{S}_k|^{1/2} (1-P_D P_G)/P_D \\ &= (2\pi)^{M/2} (CV/c_M g^M)(1-P_D P_G)/P_D \end{aligned} \tag{15}$$

The covariance update equation (8) is replaced by

$$\underline{P}_{k|k} = \underline{P}_{k|k-1} - (1-\beta_\emptyset)\underline{W}_k \underline{S}_k \underline{W}_k' + \underline{P}_k \tag{16}$$

where the data-dependent (stochastic) terms

$$\underline{P}_k \triangleq \underline{W}_k [\sum_{j=1}^{m} \beta_j \underline{\nu}_j \underline{\nu}_j' - \underline{\nu}\underline{\nu}'] \underline{W}_k' \tag{17}$$

and $\beta_\emptyset$ transform the original <u>deterministic</u> Riccati equation into a <u>stochastic</u> one.

dependence of tracking performance, particularly the behavior of $P_{k|k}$, on detection probability P_D and clutter density C. This is accomplished in the next section by means of a deterministic approximation to the stochastic Riccati equation (4) and (16).

Another major problem in data association and tracking is the testing of hypotheses for maneuver detection, track initiation, signature formation, target classification, and other decision-making purposes. The uncertainty in measurement origin leads, in the PDA and other approaches, to a modified likelihood function [18] involving the combined innovation $\underline{\nu}$ in (12). A major drawback of this approach has been the difficulty of computing the covariance matrix of $\underline{\nu}$, but this can now be done using an intermediate result to be derived in the next section.

Finally, note that multiple targets can be handled simultaneously via the joint probabilistic data association (JPDA) approach [8], in which the posterior probabilities (13)-(14) are computed jointly across a set of potentially interfering targets. Although this is a very important extension, it greatly complicates the derivations and will not be included here.

3. APPROXIMATE COVARIANCE EQUATION

Since any measure of tracking performance must depend heavily (or perhaps exclusively) on the error covariance matrix $\underline{P}_{k|k}$, we shall attempt to characterize its behavior in the presence of uncertainties in measurement origin. $\underline{P}_{k|k}$ is a random (data-dependent) matrix governed by the nonlinear, stochastic difference equations (4) and (16), and hence its behavior can only be determined in a statistical sense. Moreover, even propagation of its first and second moments appears to be intractable except via extensive numerical operations.

Consequently, we shall consider an approximation to (16) in which the random matrix $\underline{P}_k$ defined in (17) and the probability $\beta_\emptyset$ given by (14) are replaced by their (prior to time k) expected values

$$\bar{\underline{P}}_k = E\{\underline{P}_k | Y^{k-1}\} \tag{18}$$

$$\bar{\beta}_\emptyset = E\{\beta_\emptyset | Y^{k-1}\} = E\{\beta_\emptyset\} = 1 - P_D P_G \tag{19}$$

where the final expression is a consequence of $E[P\{A|B\}]=P\{A\}$.

These substitutions make (4) and (16) into a set of deterministic equations that can be iterated forward in time. Because (16) is nonlinear in $\underline{P}_{k|k-1}$, this does not yield $E\{\underline{P}_{k|k}\}$; nevertheless, it will give approximate values of future state error covariances in the presence of uncertain detections and false alarms as a function of the environmental parameters P_D and C, and of the noise covariances $\underline{R}$ and $\underline{Q}$.

Expansion of (18) yields

$$\bar{\underline{P}}_k = E\{\underline{P}_k|Y^{k-1}\} = E\{E[\underline{P}_k|m,Y^{k-1}]|Y^{k-1}\}$$

$$= \sum_{m=0}^{\infty} E[\underline{P}_k|m,Y^{k-1}]P\{m|Y^{k-1}\} \tag{20}$$

where $P\{m|Y^{k-1}\} = P\{m\}$ is given by (44) in Appendix C. Using (17) and (12), the inside expectation becomes

$$E[\underline{P}_k|m,Y^{k-1}] = \begin{cases} \underline{W}_k[\underline{U}_1(m)-\underline{U}_2(m)]\underline{W}_k', & m=1,2,\ldots \\ \\ \emptyset, & m=0 \end{cases} \tag{21}$$

where

$$\underline{U}_1(m) \triangleq E[\sum_{i=1}^{m} \beta_i \underline{\tilde{y}}_i \underline{\tilde{y}}_i'|m,Y^{k-1}] \tag{22}$$

and[3]

$$\underline{U}_2(m) \triangleq E[\sum_{i=1}^{m} \beta_i \underline{\tilde{y}}_i \sum_{j=1}^{m} \beta_j \underline{\tilde{y}}_j'|m,Y^{k-1}]$$

---

[3]The second expression in (23) is obtained as a intermediate result in Appendix D.

$$= E[\sum_{i=1}^{m} \beta_i^2 \underline{\nu}_i \underline{\nu}_i' | m, Y^{k-1}] \tag{23}$$

The expected values are obtained by multiplying the quantities in square brackets by the joint prior density $p(\underline{\nu}_1, \ldots \underline{\nu}_m | m, Y^{k-1})$ given in (49) and integrating over the validation gate.

Considerable simplifications result if one applies a linear transformation of variables ($\underline{S}_k^{-1/2}$) to obtain a spherical gate, followed by a change to spherical coordinates. Because of the spherical symmetry of the gaussian density and of the expressions (22)-(23), off-diagonal elements, cross-terms, and angular variables drop out like flies, leaving scalar integrals over the radial variables (i.e., over $||\underline{\nu}_j||$, j=1,...m). The detailed derivation, which is given in Appendix D, leads to

$$\underline{U}_1(m) = m \frac{P_D}{P_D P_G m + (1-P_D P_G) CV} \frac{c_M}{(2\pi)^{M/2}} I_1 \underline{S}_k \tag{24}$$

$$\underline{U}_2(m) = m \frac{P_D}{P_D P_G m + (1-P_D P_G) CV} \frac{c_M}{(2\pi)^{M/2}} \left(\frac{M}{g^M} \right)^{m-1} I_2(m) \underline{S}_k \tag{25}$$

where $\underline{S}_k$ is the covariance matrix of the correct innovation and the scalar integrals I_1 and $I_2(m)$ are defined as

$$I_1 \triangleq \int_0^g r^{M+1} \exp(-r^2/2) \, dr \tag{26}$$

$$I_2(m) \triangleq \int_{\emptyset}^{g} \cdots \int_{\emptyset}^{g} \frac{\exp(-r_1^2) r_1^2}{b + \sum_{j=1}^{m} \exp(-r_j^2/2)} (r_1 r_2 \cdots r_m)^{M-1} dr_1 \cdots dr_m \tag{27}$$

and the constant $b = (2\pi)^{M/2} C |\underline{S}_k|^{1/2} (1-P_D P_G)/P_D$ was defined in (15).

Substituting (24)-(27) and (44) into (2Ø) and cancelling leads to

$$\bar{\underline{P}}_k = (q_1 - q_2) \underline{W}_k \underline{S}_k \underline{W}_k' \tag{28}$$

where

$$q_1 \triangleq P_D \frac{c_M}{(2\pi)^{M/2}} \sum_{m=1}^{\infty} \frac{e^{-CV} (CV)^{m-1}}{(m-1)!} I_1 = P_D \frac{c_M}{(2\pi)^{M/2}} I_1 \tag{29}$$

$$q_2 \triangleq P_D \frac{c_M}{(2\pi)^{M/2}} \sum_{m=1}^{\infty} \frac{e^{-CV} (CV)^{m-1}}{(m-1)!} \left(\frac{M}{g^M}\right)^{m-1} I_2(m) \tag{3Ø}$$

and substitution of this and (19) into (16) yields the deterministic equation

$$\underline{P}_{k|k} = \underline{P}_{k|k-1} - (P_D P_G - q_1 + q_2) \underline{W}_k \underline{S}_k \underline{W}_k' \tag{31}$$

This can be simplified further by noting that for typical

values of g and M (g=4 or 5 and M<10), P_G is approximately 1 and q_1 is approximately P_D (substitute $x^{1/2}$ for r in I_1 to get a gamma function).

The upshot of all this is that the deterministic approximation to the covariance equation becomes

$$\underline{P}_{k|k} = \underline{P}_{k|k-1} - q_2 \underline{W}_k \underline{S}_k \underline{W}_k' \tag{32}$$

where the scalar q_2 lies between 0 and 1 and depends on P_D, C, and V, the volume of the validation region at time k. Comparing this to (8), it is clear that the factor q_2 reduces the covariance improvement due to the term $\underline{WSW}'$: the smaller q_2 is, the greater the degradation.

Since C is proportional to P_F and $V=c_M g^M |\underline{S}_k|^{1/2}$ from (11), equations (4) and (32) may be written as

$$\begin{aligned} \underline{P}_{k|k-1} &= \underline{F}\underline{P}_{k-1|k-1}\underline{F}' + \underline{G}\underline{Q}\underline{G}' \\ \underline{P}_{k|k} &= \underline{P}_{k|k-1} - q_2(\underline{S}_k; P_D, P_F)\underline{W}_k \underline{S}_k \underline{W}_k' \end{aligned} \tag{33}$$

where $\underline{W}_k$ and $\underline{S}_k$ depend upon $\underline{P}_{k|k-1}$ via (6) and (9). This modified Riccati equation describes (approximately) the behavior of the PDA tracking filter as a function of the detection and false alarm probabilities P_D and P_F. The approximation is validated via Monte Carlo simulations in Appendix E. We shall now use it to characterize the dependence of tracking performance on P_D and P_F.

For most values of P_D and P_F, (33) can be iterated until it converges to a steady-state covariance matrix $\bar{\underline{P}}(P_D,P_F)$ (the stability issue is discussed below). In order to obtain a scalar tracking performance metric, one can then extract the steady-state root-mean-square (RMS) position error

$$e(P_D,P_F) \triangleq \sqrt{\bar{p}_{11}(P_D,P_F) + \bar{p}_{22}(P_D,P_F)} \tag{34}$$

where $\bar{p}_{11}$ and $\bar{p}_{22}$ are the diagonal elements of $\bar{\underline{P}}$ that correspond to target position.

We shall refer to a contour plot of (34) as a tracker operating characteristic (TOC). This name is chosen because the well-known receiver operating characteristic (ROC) curve in the same P_D-P_F plane is the locus of possible operating points for a detector/receiver, where a particular operating point on the curve is determined by the detection threshold level. Thus, if the ROC curve is superimposed on the TOC contours, the dependence of tracking performance on detection threshold can be determined directly. This will be illustrated in the next section with an example.

There are various other performance metrics that can be used, of course, such as the determinant or trace of $\bar{\underline{P}}$. In many applications, the steady-state covariance may not be appropriate: one can instead use the value of $\underline{P}_{k|k}$ obtained by iterating (33) over a fixed period of time from a standard $\underline{P}_{\emptyset|\emptyset}$.

4. EXAMPLES

The target/sensor geometry shown in Figure 2 was used in the multi-target tracking examples of [8]. Taking the (linearized) values of $\underline{F}$, $\underline{G}$, $\underline{H}$, $\underline{Q}$, and $\underline{R}$ from the initial time in that example, we have iterated (33) to obtain the steady-state RMS position error (34) for various values of P_D and P_F. Evaluation of $q_2(\underline{S}_k; P_D, P_F)$ was carried out using a look-up procedure from tables generated off-line (see Appendix A for details).

Tracker operating characteristics will be shown for two different measurement types. In the first example, the target is tracked using measurements of bearing (azimuth) and frequency from sensors 20 and 22 at 5-minute intervals. The process noise matrix ($\underline{G}\underline{Q}\underline{G}'$) is diagonal, with standard deviations of $.2^\circ$ in course, .2 knots in speed, and .01 Hz in source frequency.

The measurement noise matrix, also diagonal, has a standard deviation of 5° in bearing and .08 Hz in frequency. We further assume that the sensor signal processing is able to resolve signals separated by about 4° and .15 Hz. We may thus view the space of bearing/frequency measurements as a collection of resolution cells, with the tracker's validation gate encompassing some subset of these cells. In practice, the detector/receiver will have an *ad hoc* rule prohibiting detections in adjacent cells, so that the *effective cell volume* is about $V_c = .3^\circ\text{-Hz}$. We assume further that false alarms occur independently in each cell with probability P_F, so that the clutter density (expected number of false alarms per unit volume) is

$$C = P_F/.3^\circ\text{-Hz} \tag{35}$$

With these assumptions, the TOC contours shown in Figure 3 have been computed (note that P_F ranges only from Ø to Ø.1). This is a contour plot of (34), with performance improving (i.e., position error decreasing) toward the upper left-hand corner. Performance degrades in the other direction, as P_D decreases and/or P_F increases, and there is a region in which the modified Riccati equation (33) does not appear to converge to a finite steady-state covariance $\underline{P}$. The question of stability is discussed further in Appendix B.

Figure 3 specifies tracking performance as a function of P_D and P_F. In order to determine what values of these probabilities are achievable, we need receiver operating characteristic (ROC) curves for the detection system that provides measurements to the tracker. To this end, we shall assume that the detection algorithm is equivalent to a set of classic quadrature receivers or incoherent matched filters [19], one operating on each resolution cell in bearing/frequency space. The quadrature receiver assumes a sinusoidal signal of unknown phase. Under the signal-plus-noise hypothesis, the test statistic has a Rician distribution, which reduces to a Rayleigh distribution in the noise-only case. Expressions for P_D and P_F may be derived [19] and used to compute the ROC curves shown in Figure 4.

For a given signal-to-noise ratio (SNR), the corresponding ROC curve is the locus of possible operating points that the detector can assume, depending on where one sets the detection threshold. In Figure 3 one such curve (SNR=8 dB) is superimposed as a dashed line on the TOC contours. This shows graphically how tracking performance depends on the operating point of the detector (i.e., on the detection threshold). In particular, performance is optimal at the operating point indicated by ⊗.

There is a relatively broad region about this point where performance is near-optimal, but performance degrades significantly thereafter.

Coherence measurements

In the second example, the target is tracked by cross-correlating signals between pairs of sensors to obtain measurements of time delay difference and Doppler difference from sensor pairs 20/21 and 21/22 (see Figure 2) at 5-minute intervals. Standard deviations of 4 sec in time difference and .004 Hz in Doppler difference are assumed, and the effective resolution cell volume is .008 sec-Hz, so that

$$C = P_F/.008 \text{ sec-Hz} \tag{36}$$

This leads to the TOC contours shown in Figure 5.

Analysis of the cross-correlation algorithm is somewhat more difficult than that of the quadrature receiver. Nevertheless, if we assume that both signal and noise are sample functions from white, gaussian, random processes and that the time-bandwidth product is 500 sec x .25 Hz, we can obtain the ROC curves shown in Figure 6. The parameter is now coherence between the two channels, rather than SNR.

Again, for a given coherence, the corresponding ROC curve is the locus of possible operating points for the coherence detector. In Figure 5, the curve corresponding to a coherence of .025 is superimposed as a dashed line on the TOC contours to show graphically how tracking performance depends on the operating

point of the coherence detector (i.e., on the detection threshold), and the optimal point is indicated by ⊗.

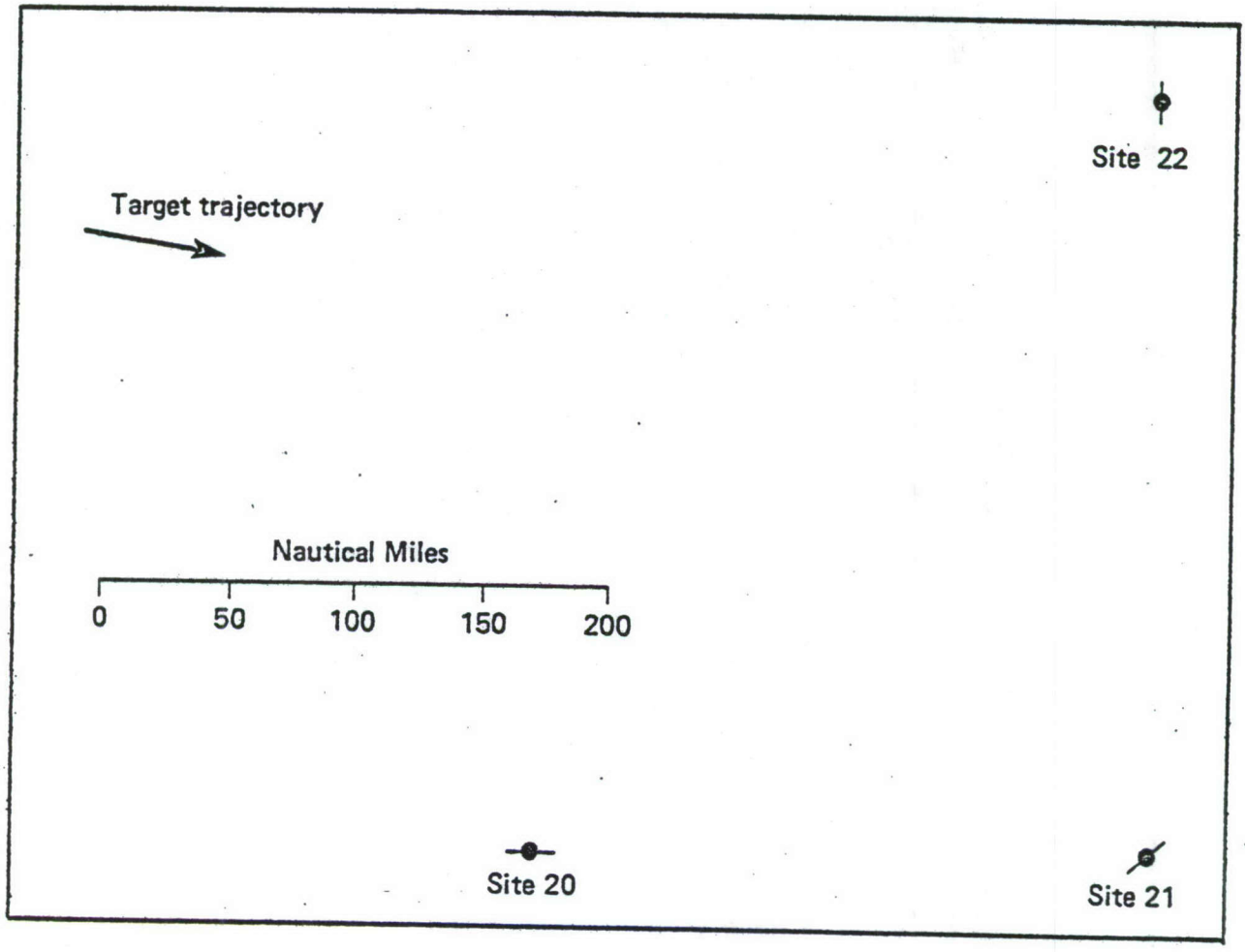

FIG. 2. TARGET-SENSOR GEOMETRY

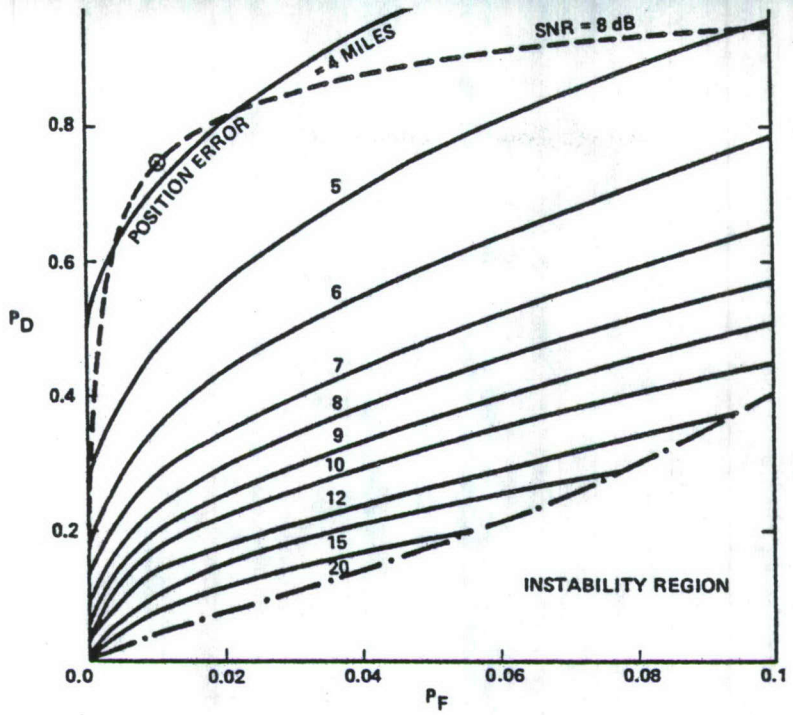

FIG. 3. TRACKER OPERATING CHARACTERISTIC (TOC) CONTOURS FOR BEARING/FREQUENCY MEASUREMENTS (DASHED LINE IS SUPERIMPOSED ROC CURVE FROM FIGURE 5)

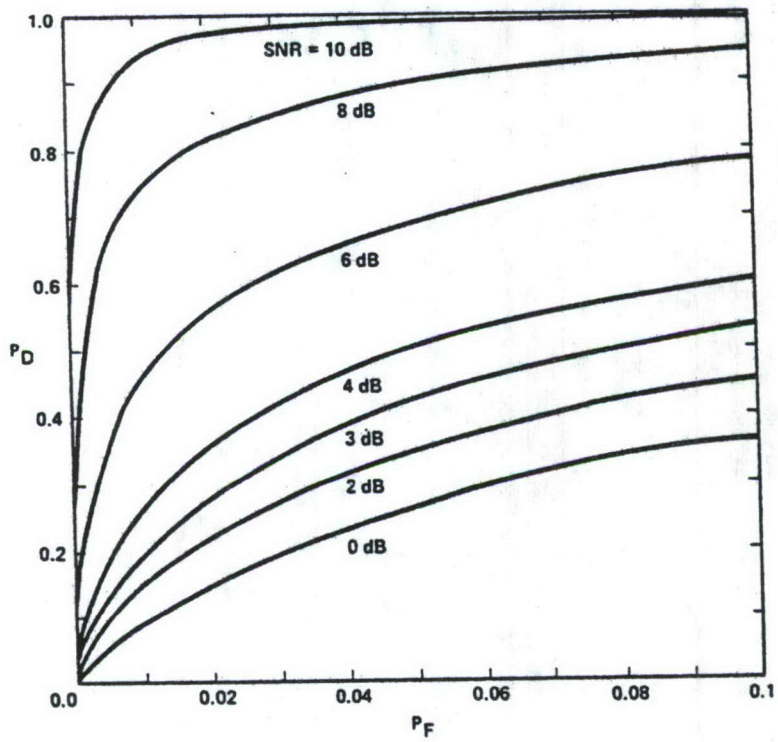

FIG. 4. ROC CURVES FOR QUADRATURE RECEIVER

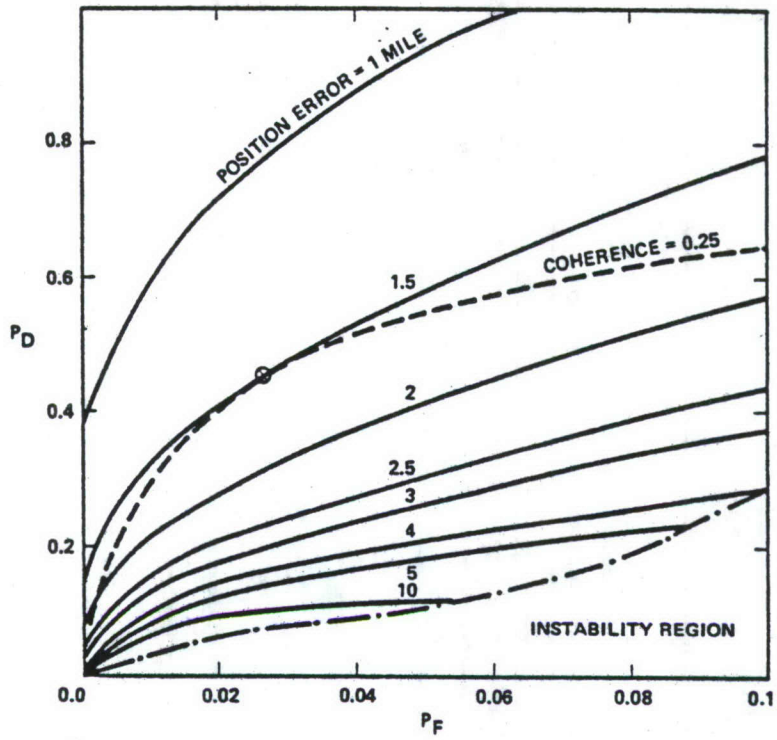

FIG. 5. TRACKER OPERATING CHARACTERISTIC (TOC) CONTOURS FOR TIME/DOPPLER DIFFERENCE MEASUREMENTS (DASHED LINE IS SUPERIMPOSE ROC CURVE FROM FIGURE 7)

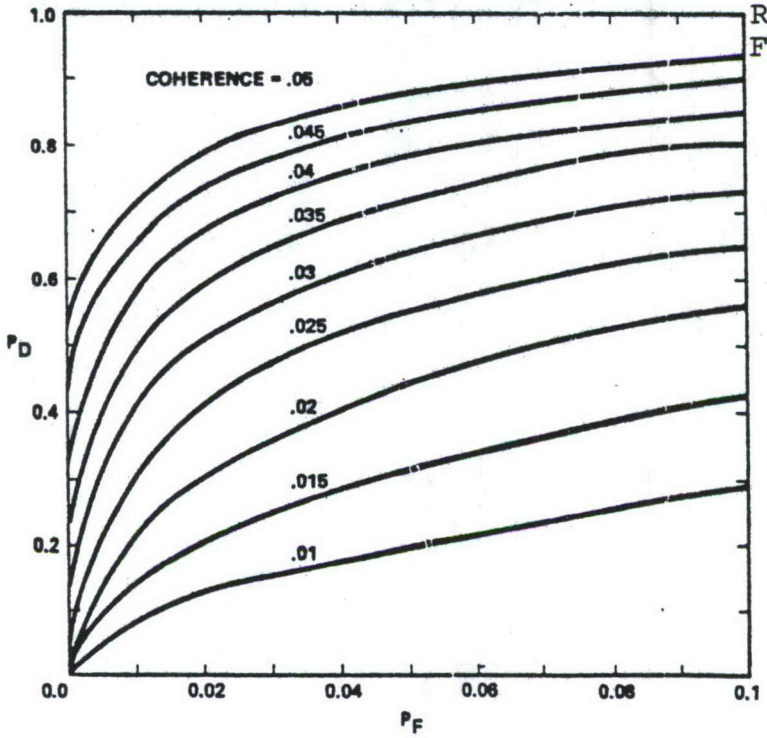

FIG. 6. ROC CURVES FOR COHERENCE RECEIVER

5. CONCLUSION

We have established, for the first time, an important relationship between thresholds in detector/receivers and performance in downstream trackers. More specifically, a modified Riccati equation determines the approximate state error covariance of a probabilistic data association (PDA) tracking filter as a function of the threshold-dependent probabilities of detection and false alarm. By plotting contours of tracking performance (in this case, steady-state RMS position error) in the P_D-P_F plane and then superimposing a ROC curve for a particular SNR, one can determine the optimal detection threshold graphically.

Several extensions of this concept are of interest. The graphical method for selecting an operating point can be replaced by a mathematical optimization: an obvious necessary condition is that the ROC and TOC curves be tangent. However, the practical difficulty of computing the required differentials to solve the necessary conditions is substantial. An approximate (e.g. table look-up) procedure for optimization would be useful for dealing with multi-dimensional TOCs, such as will occur if different receivers are allowed to have different thresholds or if bearing/frequency and time/Doppler measurements are used simultaneously.

Another issue of major importance is the optimization of tracking performance when the signal's SNR is not known. In this case, several ROC curves are involved and one must select a threshold that is best (in some sense) for a whole range of SNRs. Alternatively, an <u>adaptive thresholding</u> scheme can be devised, whereby the SNR is monitored and the threshold adjusted so as to maximize performance along the current ROC curve.

The results obtained here apply to the probabilistic data association framework, in which each target is considered individually in the presence of random clutter (false alarms). It will be useful to modify these results to deal with other data association schemes, particularly the joint PDA approach [8], in which multiple interfering targets are accounted for by computing the posterior probabilities (13)-(14) jointly across a set of targets.

A Monte-Carlo test of the validity of the key approximation, in which $\underline{P}_k$ and β_o were replaced in (16) by their expected values is presented in Appendix E, thus validating the entire ROC/TOC approach.

APPENDIX A
PROPAGATION OF THE MODIFIED RICCATI EQUATION

Propagation of the modified Riccati equation (33) requires evaluation of the scalar parameter q_2, defined by (27) and (30). This was carried out numerically as follows. First, a 50,000-point Monte-Carlo integration scheme was used repeatedly to create a table of values of the integral (27) for various values of b, m=1-15, and M=1-4 (the gate size was fixed arbitrarily at g=4). Then routines from the numerical package IMSL were used to compute spline coefficients for interpolation over b. Finally, the tables and coefficients were embedded in a subroutine that accepts values of M, P_D and CV ($=P_F V/V_c$) and evaluates (30) by truncating the sum at m=15 and using the spline interpolation to evaluate the integral.

As can be seen from (27) and (30), for a given dimension of the measurement vector, M, and gate size, g, the resulting coefficient q_2 depends only on the target detection probability, P_D, and the expected number of false measurements in the gate, CV. Thus the results obtained from the above evaluation yield "universal curves", presented in Figure 7.

With this, propagation of (33) was straightforward. However, because this form of the right-hand side of the update equation is known to have poor numerical properties, it was replaced in the computer program by the equivalent equation

$$\underline{P}_{k|k} = (1-q_2)\underline{P}_{k|k-1} + q_2[(\underline{I}-\underline{W}_k\underline{H})\underline{P}_{k|k-1}(\underline{I}-\underline{W}_k\underline{H})' + \underline{W}_k\underline{R}\underline{W}_k'] \quad (37)$$

To prove the equivalence, one may simply use the well-known identity given by (8) on the terms in square brackets.

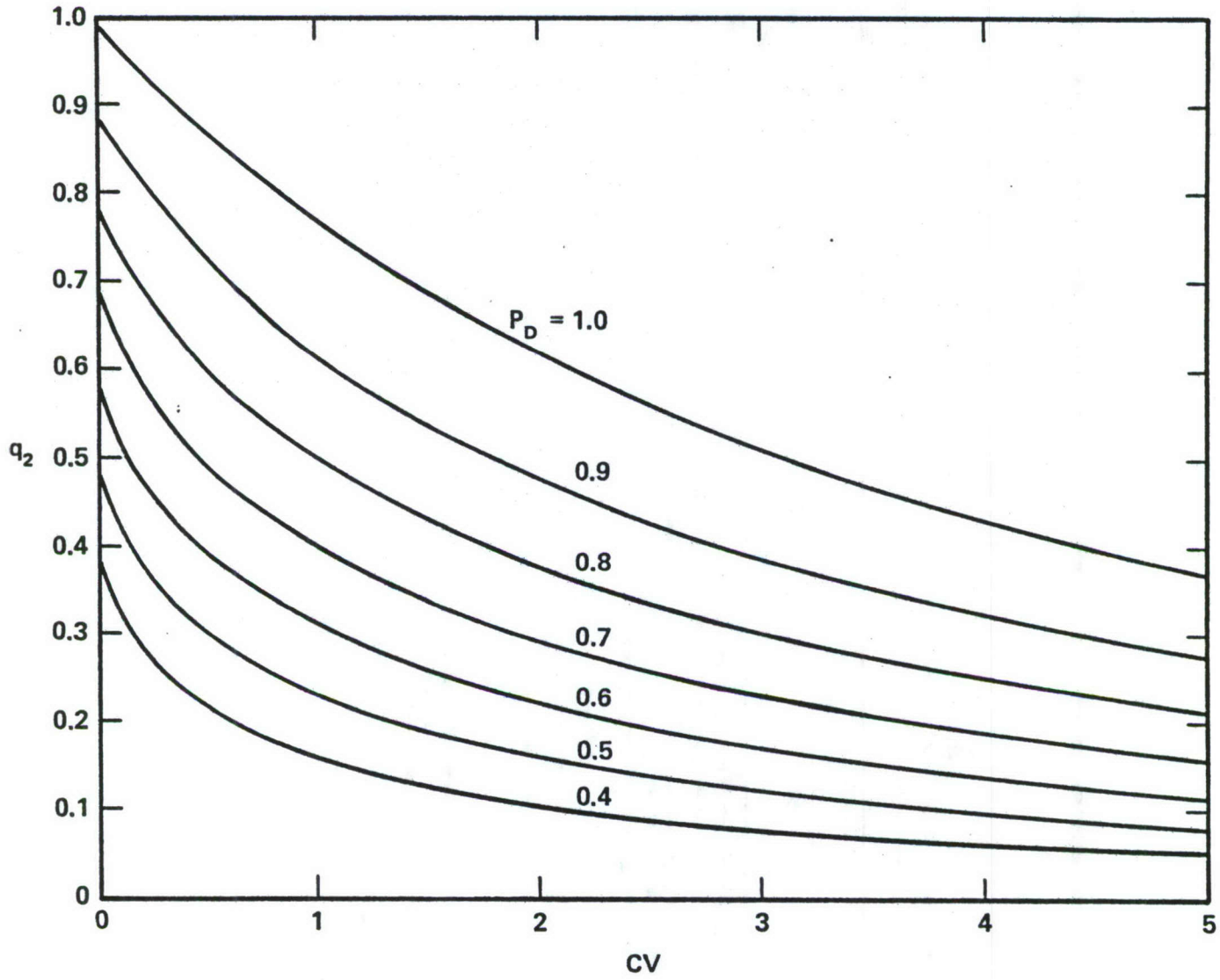

Figure 7. Factor q_2 for measurement of dimension M=2 and gate g=4

APPENDIX B
STABILITY OF THE MODIFIED RICCATI EQUATION

The standard Riccati equation defined by (4) and (8) is well-known to be stable, provided appropriate controllability and observability conditions hold [3]; it will always converge to a steady-state covariance $\bar{P}$. The modified Riccati equation (33), with an additional covariance-dependent factor q_2 on the right-hand side, presents some very challenging and unresolved stability issues. It is clear from our numerical results that (33) converges to a steady-state $\bar{P}(P_D,P_F)$ for most values of the parameters P_D and P_F. In the instability regions indicated in Figures 3 and 5, (33) diverges numerically,[4] but this does not necessarily imply that the equation is unstable in a mathematical sense.

Although we have as yet been unable to establish any general theorems on either stability or instability, examination of a scalar example provides some useful insights.

Suppose that x and y are both 1-dimensional with F=G=H=1 and Q,R>0, in which case (33) reduces to

$$P_{k+1|k} = P_{k|k-1} - q_2 P^2_{k|k-1}/[P_{k|k-1}+R] + Q \qquad (38)$$

Note that F=1 corresponds to an integrator, so that the

---

[4]Once q_2 underflows, divergence is inevitable.

covariance diverges unless it is updated.[5] If (38) converges to a steady-state value P, then we can substitute $P_{k+1|k} = P_{k|k-1} = P$ to obtain the quadratic equation

$$q_2 P^2 - QP - QR = \emptyset \tag{39}$$

which has a positive solution

$$P(q_2) = \frac{Q + \sqrt{Q^2+4QRq_2}}{2q_2} \tag{40}$$

It can be shown that for any <u>fixed</u> value of q_2 between $\emptyset$ and 1, (38) is stable and converges to (40) from any initial $P_{1|\emptyset} > \emptyset$. Indeed, we conjecture that (33) is stable for any fixed value of q_2, and that instabilities occur only because of the dependence of q_2 on P.

The stability/instability question can be illuminated for this scalar example by plotting P vs. q_2. In Figure 8, the curve labeled $P(q_2)$ has been computed from (40), while the curve labeled $q_2(P)$ has been evaluated from (30) using the subroutine described above in Appendix A, for P_D=.7 and P_F=.1. One approach to finding a steady-state solution (if one exists) of (38) is to pick an initial $P>\emptyset$ and then alternately evaluate $q_2(P)$ and $P(q_2)$, as indicated by the arrowed paths. This procedure is

---

[5]In practically all tracking problems, the plant equation contains at least one integration from velocity to position.

stable for P<800, in which case it converges to the lower intersection of the curves. For P>800, the procedure diverges as indicated, suggesting that (38) is unstable for large enough $P_{1|0}$.

Figure 9 shows the same $P(q_2)$ curve and a new $q_2(P)$ curve, computed for P_D=.2 and P_F=.1. In this case there is no point of intersection and the arrowed pathways diverge for any initial value of P.

These examples and others we have seen strongly suggest that a stable intersection is always accompanied by an unstable one at a higher value of P if P_F>0. This implies that even a small amount of clutter will render the equation unstable for sufficiently large P. We conjecture that the same statement holds for the multivariable case of (33).

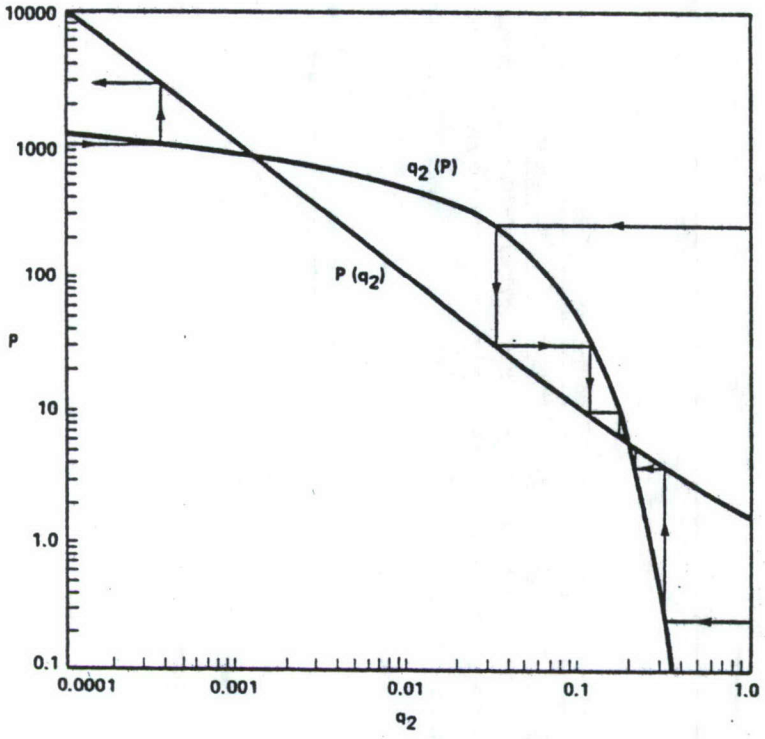

FIG. 8. STABLE AND UNSTABLE INTERSECTIONS

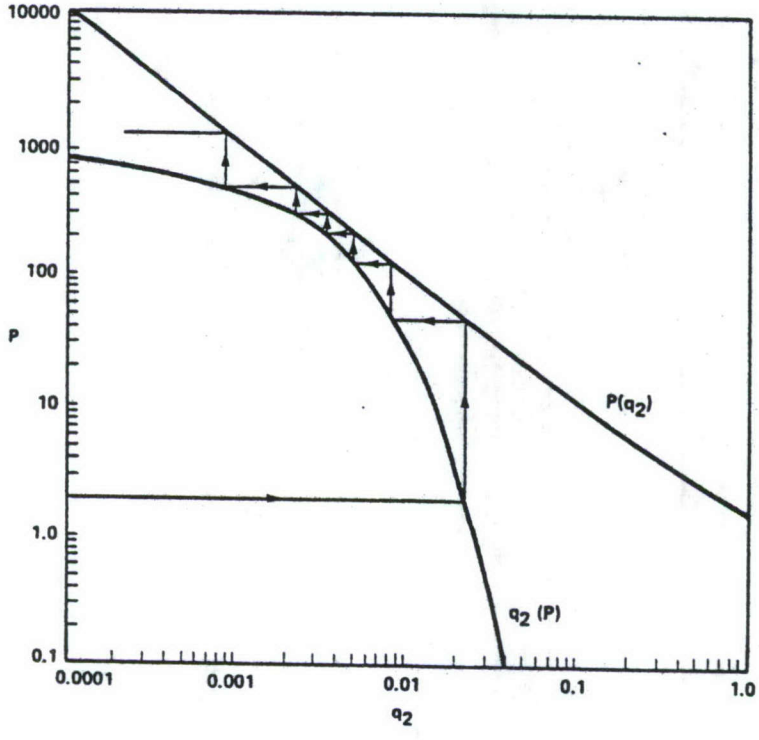

FIG. 9. UNSTABLE SITUATION

APPENDIX C
PROBABILITY CALCULATIONS

In this appendix we shall derive a number of expressions needed in the main text. Letting $\gamma_j(m)$ denote the prior probability of the event χ_j, conditioned on m, the total probability theorem yields

$$\begin{aligned}
\gamma_j(m) &= P\{\chi_j|m,Y^{k-1}\} = P\{\chi_j|m\} \\
&= P\{\chi_j|m^F=m-1,m\}P\{m^F=m-1|m\} + P\{\chi_j|m^F=m,m\}P\{m^F=m|m\} \\
&= \begin{cases} (1/m)P\{m^F=m-1|m\} + (\emptyset)P\{m^F=m|m\}, & j=1,\ldots m \\ (\emptyset)P\{m^F=m-1|m\} + (1)P\{m^F=m|m\}, & j=\emptyset \end{cases}
\end{aligned} \tag{41}$$

because m^F, the number of false measurements, must be either m-1 (if the target is detected) or m (if it is not). Using Bayes' rule and the assumed Poisson distribution for false measurements,

$$\begin{aligned}
P\{m^F=m-1|m\} &= P\{m|m^F=m-1\}P\{m^F=m-1\}/P\{m\} \\
&= [P_D P_G][e^{-CV}(CV)^{m-1}/(m-1)!]/P\{m\} \\
&= P_D P_G m/[P_D P_G m + (1-P_D P_G)CV]
\end{aligned} \tag{42}$$

$$P\{m^F=m|m\} = P\{m|m^F=m\}P\{m^F=m\}/P\{m\}$$

$$= [1-P_DP_G][e^{-CV}(CV)^m/m!]/P\{m\}$$

$$= (1-P_DP_G)CV/[P_DP_Gm + (1-P_DP_G)CV] \qquad (43)$$

where the denominator $P\{m\}$ is the prior probability of m and is equal to the sum of the numerators in the two equations:

$$P\{m\} = P\{m|Y^{k-1}\}$$

$$= [P_DP_Gm + (1-P_DP_G)CV]e^{-CV}(CV)^{m-1}/m!, \quad m=0,1,... \qquad (44)$$

Substituting back into (41) yields

$$\gamma_j(m) = \begin{cases} P_DP_G/[P_DP_Gm + (1-P_DP_G)CV], & j=1,...m \\ (1-P_DP_G)CV/[P_DP_Gm + (1-P_DP_G)CV], & j=0 \end{cases} \qquad (45)$$

Note that $\gamma_j(m)$ is independent of j for $j>0$.

Using Bayes' rule, the posterior probabilities in (12) can be expressed as

$$\beta_j \triangleq P\{\chi_j|Y^k\} = P\{\chi_j|\underline{Y}_1,...\underline{Y}_m,m,Y^{k-1}\}$$

$$= p(\underline{Y}_1,...\underline{Y}_m|\chi_j,m,Y^{k-1})P\{\chi_j|m,Y^{k-1}\}/p(\underline{Y}_1,...\underline{Y}_m|m,Y^{k-1})$$

$$= p(\underline{Y}_1,\ldots\underline{Y}_m|\chi_j,m,Y^{k-1})\,\gamma_j(m)/\sum_{j=\emptyset}^{m}\text{numerators} \tag{46}$$

The first factor is the joint probability density of the m candidate measurements, conditioned on the j-th one being correct. According to the PDA assumptions, the correct measurement $\underline{Y}_j$ has a gaussian density

$$N(\underline{Y}_j;\underline{\emptyset},\underline{S}_k)/P_G \triangleq (1/P_G)\exp(-\underline{Y}_j'\underline{S}^{-1}\underline{Y}_j/2)/(2\pi)^{M/2}|\underline{S}_k|^{1/2} \tag{47}$$

with mean $\underline{\emptyset}$ and covariance $\underline{S}_k$, where the factor $1/P_G$ accounts for its restriction to the validation gate, and each incorrect measurement has a uniform density V^{-1}. It follows that

$$p(\underline{Y}_1,\ldots\underline{Y}_m|\chi_j,m,Y^{k-1}) = \begin{cases} V^{-m+1}N(\underline{Y}_j;\underline{\emptyset},\underline{S}_k)/P_G, & j=1,\ldots m \\ V^{-m}, & j=\emptyset \end{cases} \tag{48}$$

The second factor in (46) is the prior probability of χ_j, given by (45). The denominator is the <u>joint prior density</u> of the measurements, conditioned only on m (and the past data),

$$p(\underline{Y}_1,\ldots\underline{Y}_m|m,Y^{k-1}) = \tag{49}$$

$$V^{-m}\gamma_{\emptyset}(m) + V^{-m+1}\sum_{j=1}^{m}(1/P_G)N(\underline{Y}_j;\underline{\emptyset},\underline{S}_k)\,\gamma_j(m)$$

Note that with the above conditioning, the validated measurements are not independent, i.e., (49) is not equal to the product over j of the marginal prior densities

$$p(\underline{Y}_j|m,Y^{k-1}) = V^{-1}[1-\gamma_j(m)] + (1/P_G)N(\underline{Y}_j;\underline{\emptyset},\underline{S}_k)\gamma_j(m) \qquad (50)$$

Finally, substitution of (45), (48), and (49) into (46) followed by a certain amount of rearrangement yields

$$\beta_j = \frac{\exp(-\underline{Y}_j'\underline{S}_k^{-1}\underline{Y}_j/2)}{b + \sum_{i=1}^{m}\exp(-\underline{Y}_i'\underline{S}_k^{-1}\underline{Y}_i/2)}, \qquad j=1,\ldots m \qquad (51)$$

$$\beta_\emptyset = \frac{b}{b + \sum_{i=1}^{m}\exp(-\underline{Y}_i'\underline{S}_k^{-1}\underline{Y}_i/2)} \qquad (52)$$

where

$$b \triangleq (2\pi)^{M/2}C|\underline{S}_k|^{1/2}(1-P_DP_G)/P_D$$
$$= (2\pi)^{M/2}(CV/c_Mg^M)(1-P_DP_G)/P_D \qquad (53)$$

APPENDIX D.
DERIVATION OF THE U_1 AND U_2 INTEGRALS

In this appendix the expectations

$$\underline{U}_1(m) \triangleq E\left[\sum_{i=1}^{m} \beta_i \tilde{\underline{y}}_i \tilde{\underline{y}}_i' \,|\, m, Y^{k-1}\right] \tag{54}$$

and

$$\underline{U}_2(m) \triangleq E\left[\sum_{i=1}^{m} \beta_i \tilde{\underline{y}}_i \sum_{j=1}^{m} \beta_j \tilde{\underline{y}}_j' \,|\, m, Y^{k-1}\right] \tag{55}$$

will be evaluated, where β_i is given by (13)-(14) and the joint density of $\tilde{\underline{y}}_1, \ldots \tilde{\underline{y}}_m$ is (48). In order to simplify the arguments, we shall make use of the fact that $\underline{S}_k$ is positive definite and change variables to

$$\underline{\zeta}_i = \underline{S}_k^{-\frac{1}{2}} \tilde{\underline{y}}_i \,, \quad i = 1, \ldots m \tag{56}$$

so that

$$\tilde{\underline{y}}_i' \underline{S}_k^{-1} \tilde{\underline{y}}_i = \underline{\zeta}_i' \underline{\zeta}_i = \|\underline{\zeta}_i\|^2 \tag{57}$$

and

$$\tilde{\underline{y}}_i \tilde{\underline{y}}_i' = \underline{S}_k^{\frac{1}{2}} \underline{\zeta}_i \underline{\zeta}_i' \underline{S}_k^{\frac{1}{2}} \tag{58}$$

In terms of the new variables $\underline{\zeta}_i$, the validation gate becomes a sphere $\{\underline{\zeta} : \|\underline{\zeta}\|^2 \leq g^2\}$ with volume $c_M g^M \triangleq \hat{V}$; the β_i's can be rewritten as

$$\hat{\beta}_i = \frac{e^{-\frac{1}{2}\|\underline{\zeta}_i\|^2}}{b + \sum_{j=1}^{m} e^{-\frac{1}{2}\|\underline{\zeta}_j\|^2}}, \quad i = 1,\ldots m \tag{59}$$

where

$$b \triangleq (2\pi)^{M/2}(CV/c_M g^M)(1-P_D P_G)/P_D \tag{60}$$

is the same as in (15). Note that the dimensionless quantity CV, the average number of false measurements in the (now spherical) gate, is unaffected by the variable change. The joint density (49) becomes

$$p(\underline{\zeta}_1,\ldots\underline{\zeta}_m|m,Y^{k-1}) = \gamma_0(m)\hat{V}^{-m} + \gamma_j(m)\hat{V}^{-m+1} \sum_{i=1}^{m} N(\underline{\zeta}_i;\underline{0},\underline{I})/P_G \tag{61}$$

if $\|\underline{\zeta}_i\| \leq g$ for all i, and 0 otherwise.

Using the change of coordinates from $\tilde{\underline{y}}$ to $\underline{\zeta}$, expressions (21) through (23) may be reexpressed as follows:

$$E[\underline{P}_k|m,Y^{k-1}] = \underline{W}\underline{S}_k^{\frac{1}{2}}[\hat{\underline{U}}_1(m)-\hat{\underline{U}}_2(m)]\underline{S}_k^{\frac{1}{2}}\underline{W}', \quad m=1,2,\ldots \tag{62}$$

$$\hat{\underline{U}}_1(m) = E[\sum_{i=1}^{m}\hat{\beta}_i\underline{\zeta}_i\underline{\zeta}_i'|Y^{k-1},m] = \underline{S}_k^{-\frac{1}{2}}\underline{U}_1(m)\underline{S}_k^{-\frac{1}{2}} \tag{63}$$

$$\hat{\underline{U}}_2(m) = E[\sum_{i=1}^{m}\hat{\beta}_i\underline{\zeta}_i\sum_{j=1}^{m}\hat{\beta}_j\underline{\zeta}_j'|Y^{k-1},m] = \underline{S}_k^{-\frac{1}{2}}\underline{U}_2(m)\underline{S}_k^{-\frac{1}{2}} \tag{64}$$

Let D stand for the spherical validation gate region. Then the above two expectations may be written out explicitly as multiple integrals of certain matrices, taken over m copies of D:

$$\hat{\underline{U}}_1 = \int_D\int_D\cdots\int_D \underline{A}(\underline{\zeta}_1,\ldots,\underline{\zeta}_m)p(\underline{\zeta}_1,\ldots,\underline{\zeta}_m)d\underline{\zeta}_1\ldots d\underline{\zeta}_m \tag{65}$$

$$\hat{\underline{U}}_2 = \int_D\int_D\cdots\int_D \underline{B}(\underline{\zeta}_1,\ldots,\underline{\zeta}_m)p(\underline{\zeta}_1,\ldots,\underline{\zeta}_m)d\underline{\zeta}_1\ldots d\underline{\zeta}_m \tag{66}$$

where p is the joint innovations density (61) with the conditioning suppressed and $\underline{A},\underline{B}$ are M×M matrices described componentwise by

$$A_{pq} = \sum_{i=1}^{m}\hat{\beta}_i\zeta_i^p\zeta_i^q \qquad 1 \le p,q \le M \tag{67}$$

$$B_{pq} = \sum_{i,j=1}^{m}\hat{\beta}_i\hat{\beta}_j\zeta_i^p\zeta_j^q \qquad 1 \le p,q \le M \tag{68}$$

Here the M-dimensional vector $\underline{\zeta}_k$ has been denoted as $(\zeta_k^1, \zeta_k^2, \ldots, \zeta_k^M)$. The integrals (65) and (66) are actually mM-fold integrals. Although the complexity of undertaking such a large computation directly would prove formidable, a number of observations show that these integrals have a fairly simple and straightforward structure:

Observation 1. The matrices $\hat{\underline{U}}_1$ and $\hat{\underline{U}}_2$ are diagonal.

From the expressions (67) and (68) one may deduce that off-diagonal elements will integrate out to zero. For when $p \neq q$, both A_{pq} and B_{pq} become odd polynomials of second degree in the variables $\zeta_1^1, \ldots, \zeta_m^M$, with coefficients either single $\hat{\beta}$'s or pairwise products of $\hat{\beta}$'s. Now both the $\hat{\beta}$'s and the two terms of the probability density p in (61) are positive functions depending only on $||\underline{\zeta}_1||, \ldots, ||\underline{\zeta}_m||$, i.e. they have the same values at antipodal points of a sphere. The odd polynomials from A_{pq} and B_{pq} will have opposite values at antipodal points, so that their contributions to the total integral will cancel.

Physically, this amounts to the observation that off-diagonal elements of the inertia tensor vanish in a principal axis system, for a spherical body with the shape of the validation region and with mass distribution density appropriately defined in terms of the $\hat{\beta}$'s and p.

Observation 2. Integrals of cross terms ($i \neq j$) vanish in the sum (68) defining B_{pq}.

From the previous observation, we need only concern ourselves with diagonal entries B_{pp}. Again when $i \neq j$ we have an odd polynomial in the $\underline{\zeta}$'s, and the same arguments as before apply again to show its integral over a sphere, weighted by the density p, must vanish.

From the point of view of the original definition (64) of $\hat{\underline{U}}_2$, we could say that distinct innovations $\underline{\zeta}_i, \underline{\zeta}_j$ are orthogonal: their inner products vanish and do not contribute to the second moment of the combined innovations.

Observation 3. Each term of $\underline{A}$ or $\underline{B}$ making a nonvanishing contribution to $\hat{\underline{U}}_N$, N=1 or 2, has the same value, given explicitly by

$$\eta_N = K \int_0^\sigma \cdots \int_0^\sigma \left[\frac{e^{-\frac{1}{2}r_1^2}}{b + \sum_{j=1}^m e^{-\frac{1}{2}r_j^2}} \right]^N \left(C_g \sum_{j=1}^m e^{-\frac{1}{2}r_j^2} + C_u \right) r_1^2 \left(\prod_{j=1}^m r_j \right)^{M-1} dr_1 \cdots dr_m \tag{69}$$

where

$$C_g = C_g(m,M) \triangleq \frac{\gamma_j(m)}{(2\pi)^{M/2} (c_M g^M)^{m-1} P_G} \tag{70}$$

$$C_u = C_u(m,M) \triangleq \frac{\gamma_0(m)}{(c_M g^M)^m} \tag{71}$$

$$K = K(m,M) = M^{m-1} c_M^m \tag{72}$$

To prove this, let us consider the first term of the (1,1) entry of each integral, which can be written as $\hat{\beta}_1^N (\zeta_1^1)^2 p(\underline{\zeta}_1, \ldots, \underline{\zeta}_m)$, N=1,2. Since p and $\hat{\beta}_1$ depend only on the norms $\|\underline{\zeta}_i\| = r_i$, it is clearly advantageous to introduce spherical coordinates in each of the m copies of the $\underline{\zeta}$-space:

$$d\underline{\zeta}_i = d\zeta_i^1 d\zeta_i^2 \ldots d\zeta_i^M = r_i^{M-1} dr_i d\omega_i^{M-1} \tag{73}$$

Here $d\omega_i^{M-1}$ denotes the "unit solid angle," i.e. the surface element on the unit sphere $(\zeta_i^1)^2 + (\zeta_i^2)^2 + \ldots + (\zeta_i^M)^2 = 1$.

Making these substitutions, the integral for the expected value of $\hat{\beta}_1^N (\zeta_1^1)^2$ becomes

$$\int_0^\sigma \cdots \int_0^\sigma \left[\frac{e^{-\frac{1}{2}r_1^2}}{b + \sum_{j=1}^m e^{-\frac{1}{2}r_j^2}} \right]^N (\zeta_1^1)^2 \left(C_g \sum_{j=1}^m e^{-\frac{1}{2}r_j^2} + C_u\right) (r_1^{M-1} dr_1 d\omega_1^{M-1}) \ldots (r_m^{M-1} dr_m d\omega_m^{M-1}) \tag{74}$$

The constants C_g, C_u, and K defined in (70) , (71) are introduced to simplify the notation.

The expression in (74) is not yet complete because the variable ζ_1^1 still has to be reexpressed in angular ω_1-coordinates for the first copy of the M-dimensional state space. However, the other angular variables $\omega_2^{M-1},\ldots,\omega_m^{M-1}$ do not occur in the integrand, so that their integrals can be absorbed in the constant K. The fact needed to do this is that the integral of the unit solid angle is just the surface area of the unit sphere, which is M times c_M (the volume of the unit sphere).

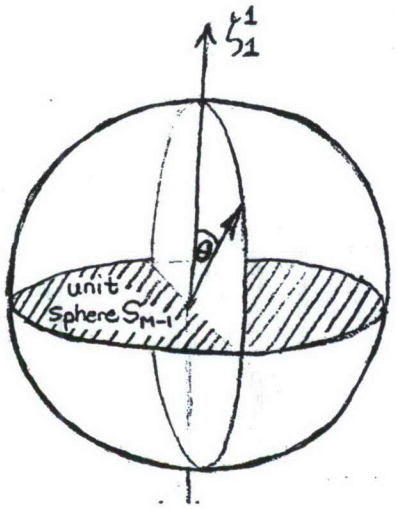

Figure 10. Unit sphere S_M

To handle the ζ_1^1-dependence of the integrand in (74) we are going to use an argument almost identical to the one used to derive the volume of the unit sphere (which is to start from a known integral and "work backwards"). The known integral that we wish to exploit is

$$\int_{\mathbb{R}_M} (\zeta_1^1)^2 \exp(-\tfrac{1}{2}\sum_{j=1}^{M}\zeta_j^2)\, d\zeta_1^1 d\zeta_1^2 \ldots d\zeta_1^M = (2\pi)^{M/2} \qquad (75)$$

Now if this integral is rewritten in spherical coordinates, we should make a substitution $\zeta_1^1 = r_1 f(\omega_1^{M-1})$ where f is a smooth function independent of r_1. For example if coordinates are chosen on the sphere as depicted in Figure 10, we would have $f(\omega_1^{M-1}) = \cos\theta$, where the angle θ is measured downward from the north pole as shown. Rewriting (75) in spherical coordinates gives

$$(2\pi)^{M/2} = \int_0^\infty r_1^2 e^{-\frac{1}{2}r_1^2}\, r_1^{M-1}\, dr_1 \int_{\substack{\text{sphere} \\ r_1 \equiv 1}} f^2(\omega_1^{M-1})\, d\omega_1^{M-1} \tag{76}$$

The substitution $\frac{1}{2}r_1^2 = x_1$ transforms the radial part of (75) into the well-known integral representation for the gamma function

$$\Gamma(t) = \int_0^\infty e^{-x_1}\, x_1^{t-1} dx_1 \tag{77}$$

so now we have

$$(2\pi)^{M/2} = 2^{M/2}\Gamma\left(\frac{M}{2} + 1\right) \int_{\substack{\text{sphere} \\ r_1 = 1}} f^2(\omega_1^{M-1})\, d\omega_1^{M-1} \tag{78}$$

We are now in a position to solve for the nonradial part of the integral in (78). But when this is done, the quantity we obtain is recognized to be c_M, the volume of the unit sphere:

$$\int f^2(\omega_1^{M-1})\, d\omega_1^{M-1} = \frac{\pi^{M/2}}{\Gamma(\frac{M}{2}+1)} = c_M \tag{79}$$

Actually, by using properties of the gamma function, this expression for c_M can be written more explicitly as

$$c_M = \frac{2\pi}{M} c_{M-2} = \begin{cases} \dfrac{2^{M/2}\pi^{M/2}}{M(M-2)\ldots 4\cdot 2} = \dfrac{\pi^{M/2}}{(M/2)!} & \text{if } M \text{ is even} \\ \dfrac{2^{(M+1)/2}\,\pi^{(M-1)/2}}{M(M-2)\ldots 5\cdot 3\cdot 1} & \text{if } M \text{ is odd} \end{cases} \tag{80}$$

Now returning to the original integral (74), we note that even though the integrand is <u>not</u> the same as (75), the angular dependence <u>is</u>, so that (79) may be applied. Absorbing this c_M into K shows that the $\beta_1^N(\zeta_1^1)^2$-contribution to $\hat{U}_N$ is given exactly by (69). It should be noted that this formula is also immediately valid for M=1 without even introducing the spherical change of coordinates (73), since the volume of the unit interval is 2 (correctly given by (80).

Although we began the discussion by considering the contribution of a single term $\hat{\beta}_1^N(\zeta_1^1)^2$ to the expectation, the

homogeneity of the expression (74) shows that the other terms $\hat{\beta}_1^N(\zeta_1^2)^2,\ldots,\hat{\beta}_M^N(\zeta_1^M)^2$ in the (1,1)-entry will each make an identical contribution. The same argument applies to other diagonal entries of $\hat{\underline{U}}_1$ and $\hat{\underline{U}}_2$: homogeneity again shows that each term will make the same contribution, given by (69). This justifies the conclusion that

$$\hat{\underline{U}}_N = m\eta_N\underline{I} \tag{81}$$

where $\underline{I}$ is the identity matrix.

Next, let us transform back from $\underline{\zeta}$-coordinates to the original $\underset{\sim}{y}$-coordinates as given in (58). We have proven that our original expectations $\underline{U}_1,\underline{U}_2$ are scalar multiples of the covariance matrix $\underline{S}$:

$$\underline{U}_N = \underline{S}^{\frac{1}{2}}(m\eta_N\underline{I})\underline{S}^{\frac{1}{2}} = m\eta_N\underline{S} \tag{82}$$

Finally, substitution of (70)-(72) and (45) into (69) followed by numerous cancellations yields the expressions (24)-(27) in Section 3.

APPENDIX E

VALIDATION OF THE MODIFIED RICCATI EQUATION

A set of Monte Carlo simulations was performed to validate the result of the modified (deterministic) approximation (33) of the stochastic Riccati equation (16).

The following notations are used:

- $\underline{P}(k|k)$ - The PDAF-calculated conditional error covariance from the stochastic Riccati equation (a random matrix, different from run to run)
- $E\{\underline{P}(k|k)\}$ - The Monte Carlo average of the above
- $\underline{P}^t(k|k)$ - The true covariance of the PDAF estimation error (different from run to run)
- $E\{\underline{P}^t(k|k)\}$ - The Monte Carlo average of the above
- $\underline{P}^d(k|k)$ - The result of the modified (deterministic) approximation (33) of the stochastic Riccati equation

The results are for the numerical problem specified in [8]. where targets were tracked in two-dimensional geographic space. The sample means were computed from ten independent runs. The scalar performance measures used in comparing the matrices $\underline{P}^d$, $E\{\underline{P}\}$ and $E\{\underline{P}^t\}$ were

$$\text{R.M.S. error} = \sqrt{tr(\underline{P})} \tag{83}$$

$$\text{R.M.S. position error} = \sqrt{P_{11} + P_{12}} \tag{84}$$

Figures 11 - 18 present the error comparison using the above two scalar measures for up to 200 time steps and a wide

range of P_D, P_F. The actual position error was closely approximated by the modified Riccati equation even for the very low $P_D = .3$. The overall error was still reasonably well approximated down to $P_D = .4$.

It appears, therefore, that the modified Riccati equation can be considered as a reliable design tool except for the situation of very low P_D.

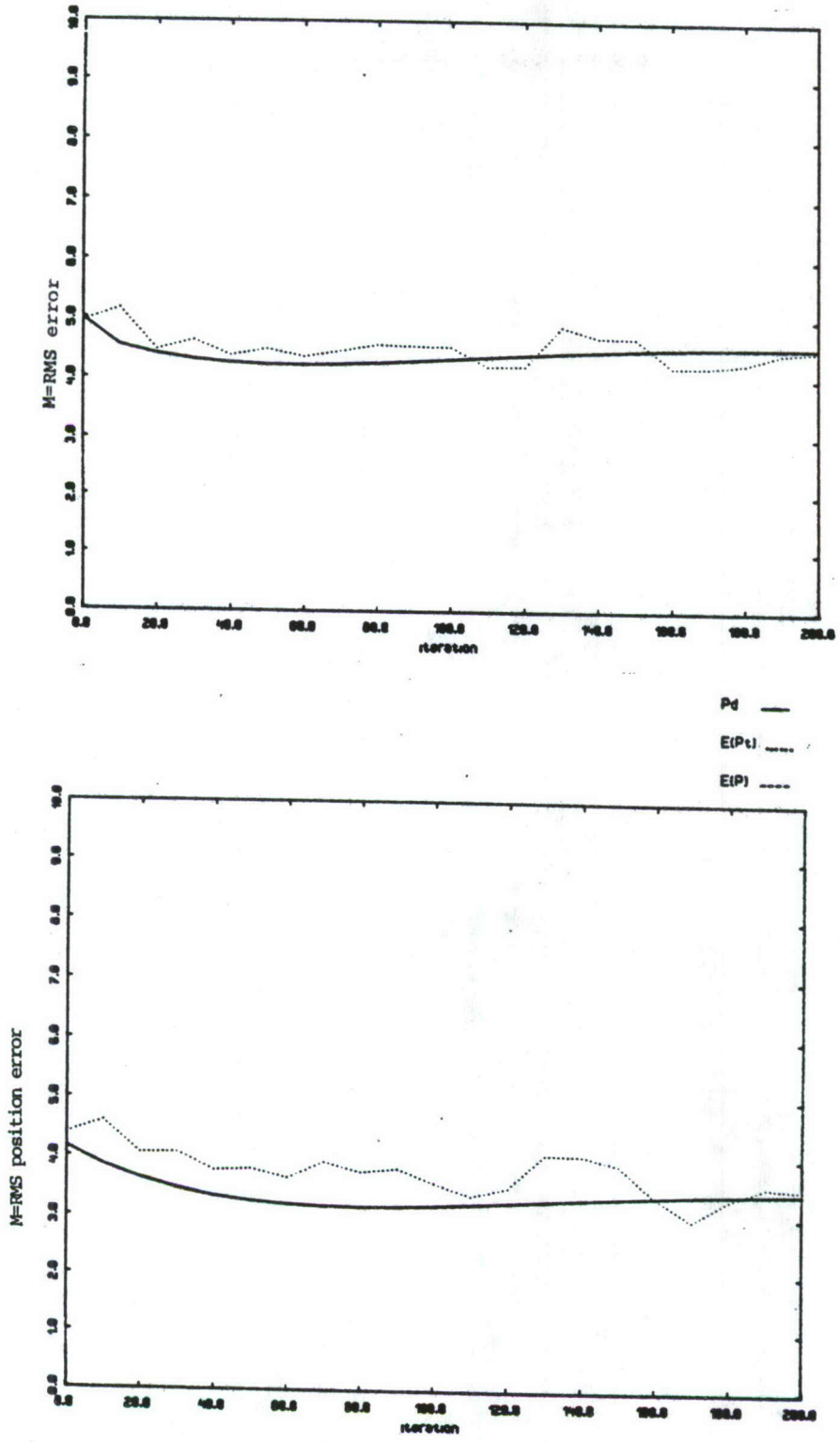

Figure 11. $M \cdot P^{d}_{k|k}$, $M \cdot E\{P^{t}_{k|k}\}$, and $M \cdot E\{P_{k|k}\}$ for $(P_D, P_F) = (1, 0)$

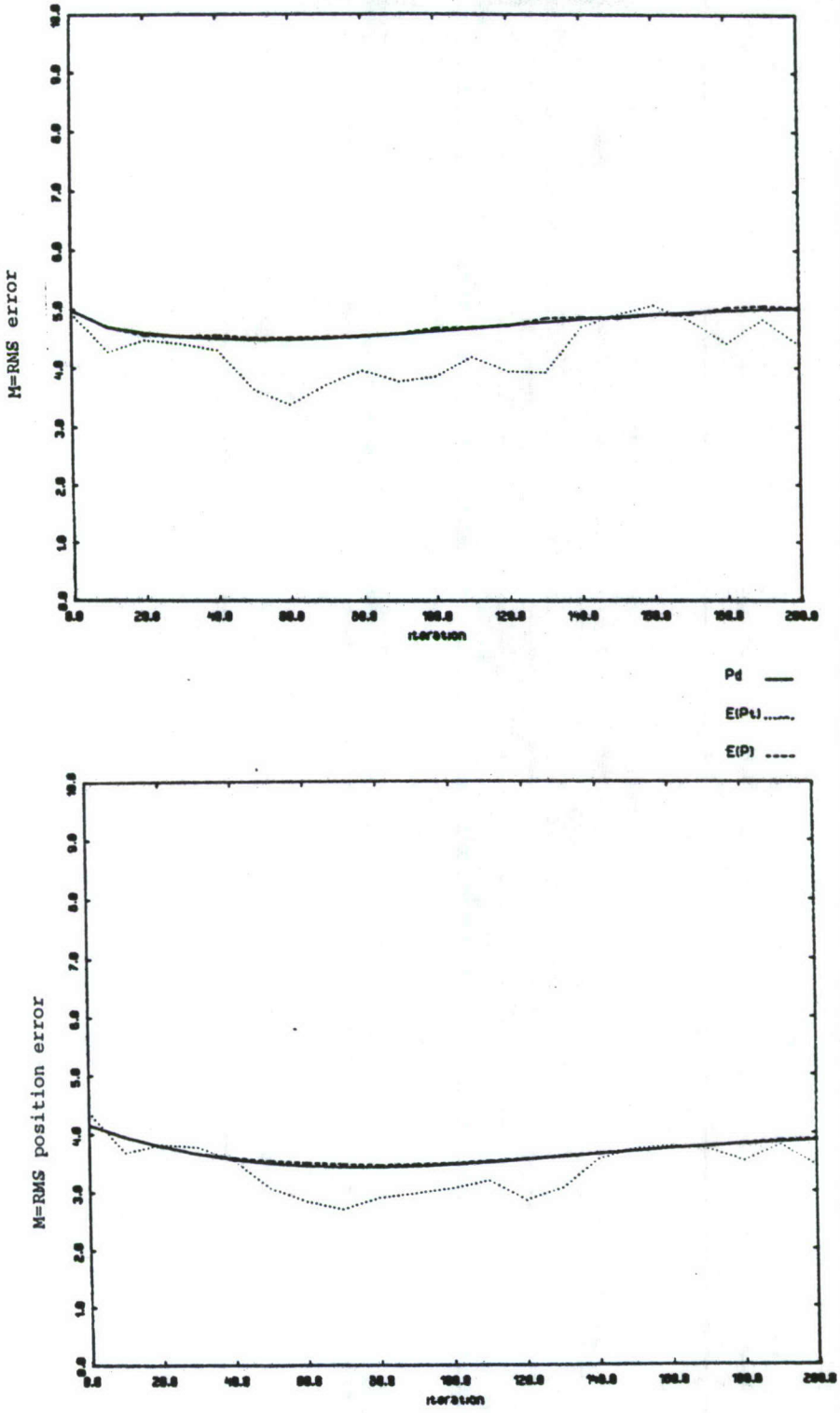

Figure 12. $M \cdot \underline{P}^{d}_{k|k}$, $M \cdot E\{\underline{P}^{t}_{k|k}\}$, and $M \cdot E\{\underline{P}_{k|k}\}$ for $(P_D, P_F) = (.9, .01)$

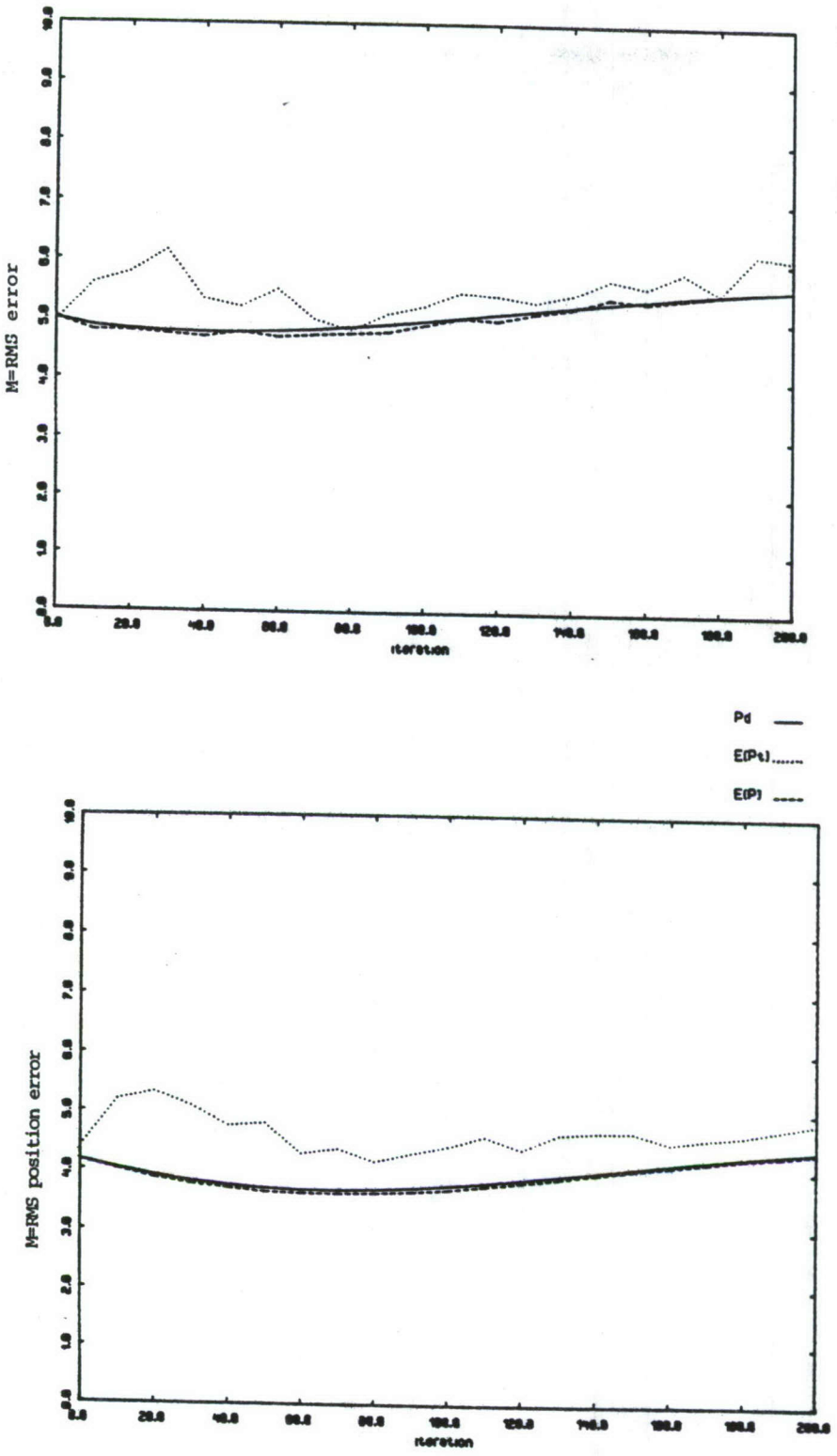

Figure 13. $M \cdot \underline{P}^{d}_{k|k}$, $M \cdot E\{\underline{P}^{t}_{k|k}\}$, and $M \cdot E\{\underline{P}_{k|k}\}$ for $(P_D, P_F) = (.8, .02)$

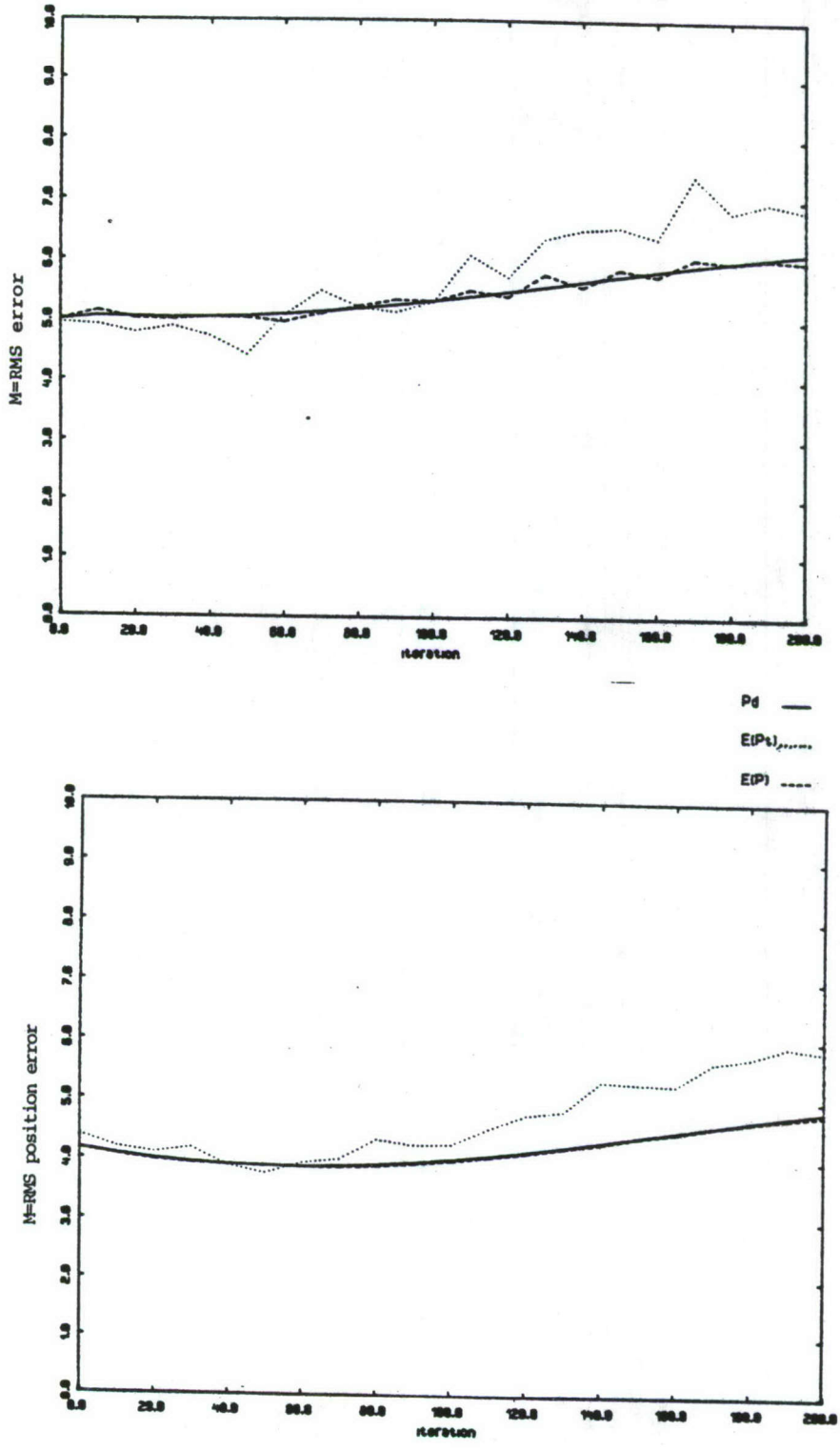

Figure 14. $M \cdot \underline{P}^{d}_{k|k}$, $M \cdot E\{\underline{P}^{t}_{k|k}\}$, and $M \cdot E\{\underline{P}_{k|k}\}$ for $(P_D, P_F) = (.7, .03)$

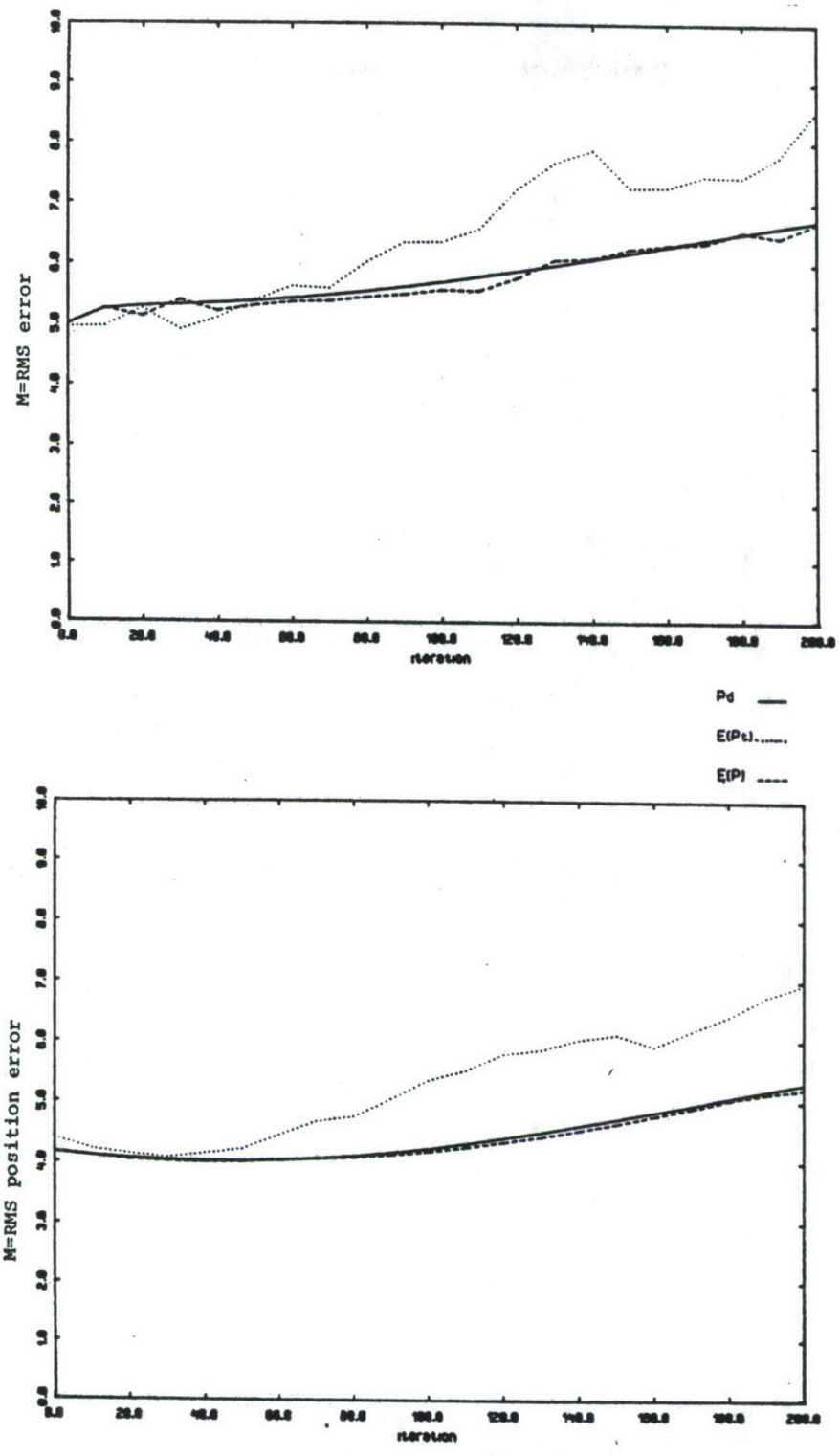

Figure 15. $M^{\cdot}P^{d}_{k|k}$, $M^{\cdot}E\{P^{t}_{k|k}\}$, and $M^{\cdot}E\{P_{k|k}\}$ for $(P_D,P_F) = (.6,.04)$

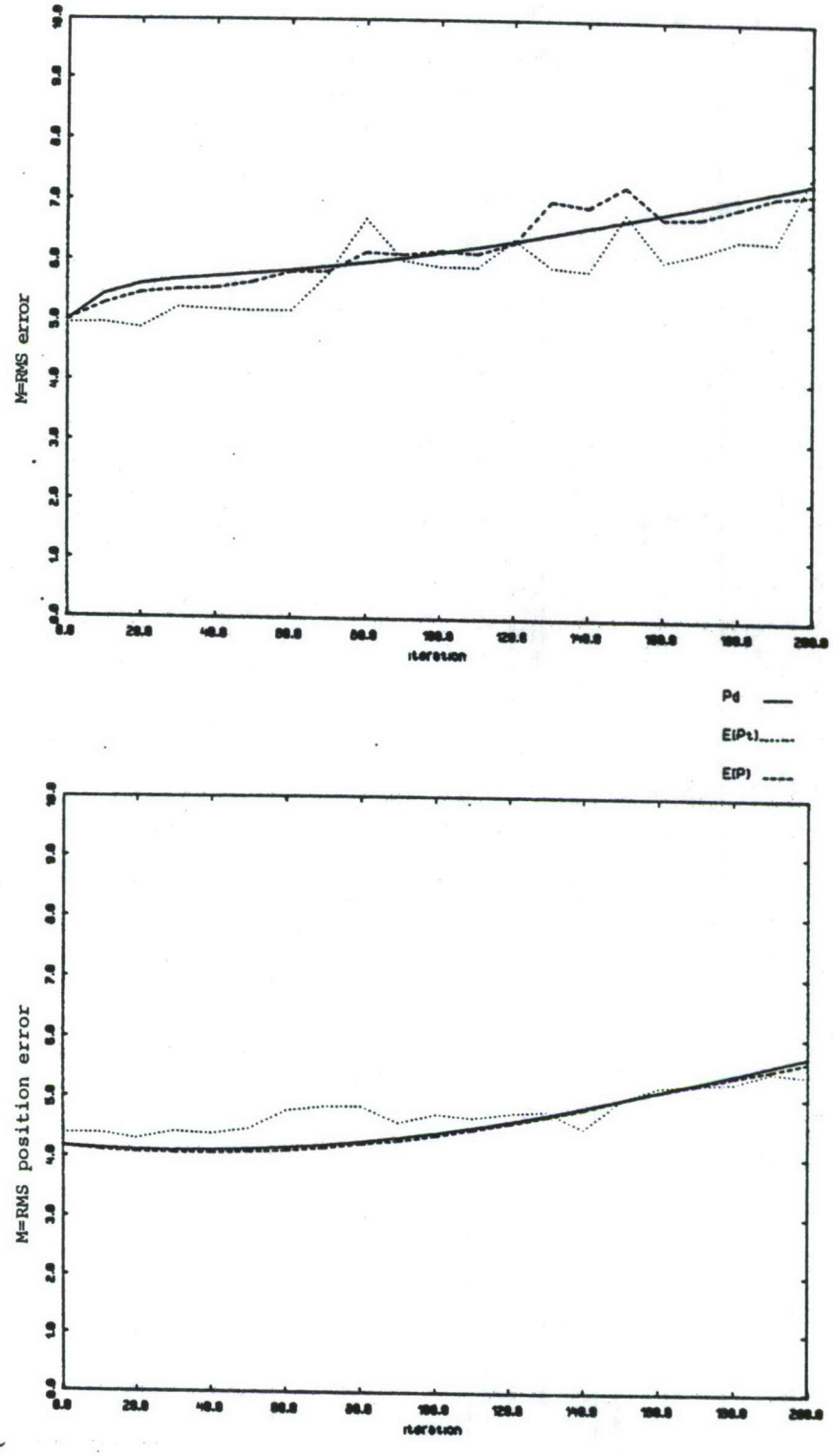

Figure 16. $M \cdot P^{d}_{k|k}$, $M \cdot E\{P^{t}_{k|k}\}$, and $M \cdot E\{P_{k|k}\}$ for $(P_D, P_F) = (.5, .05)$

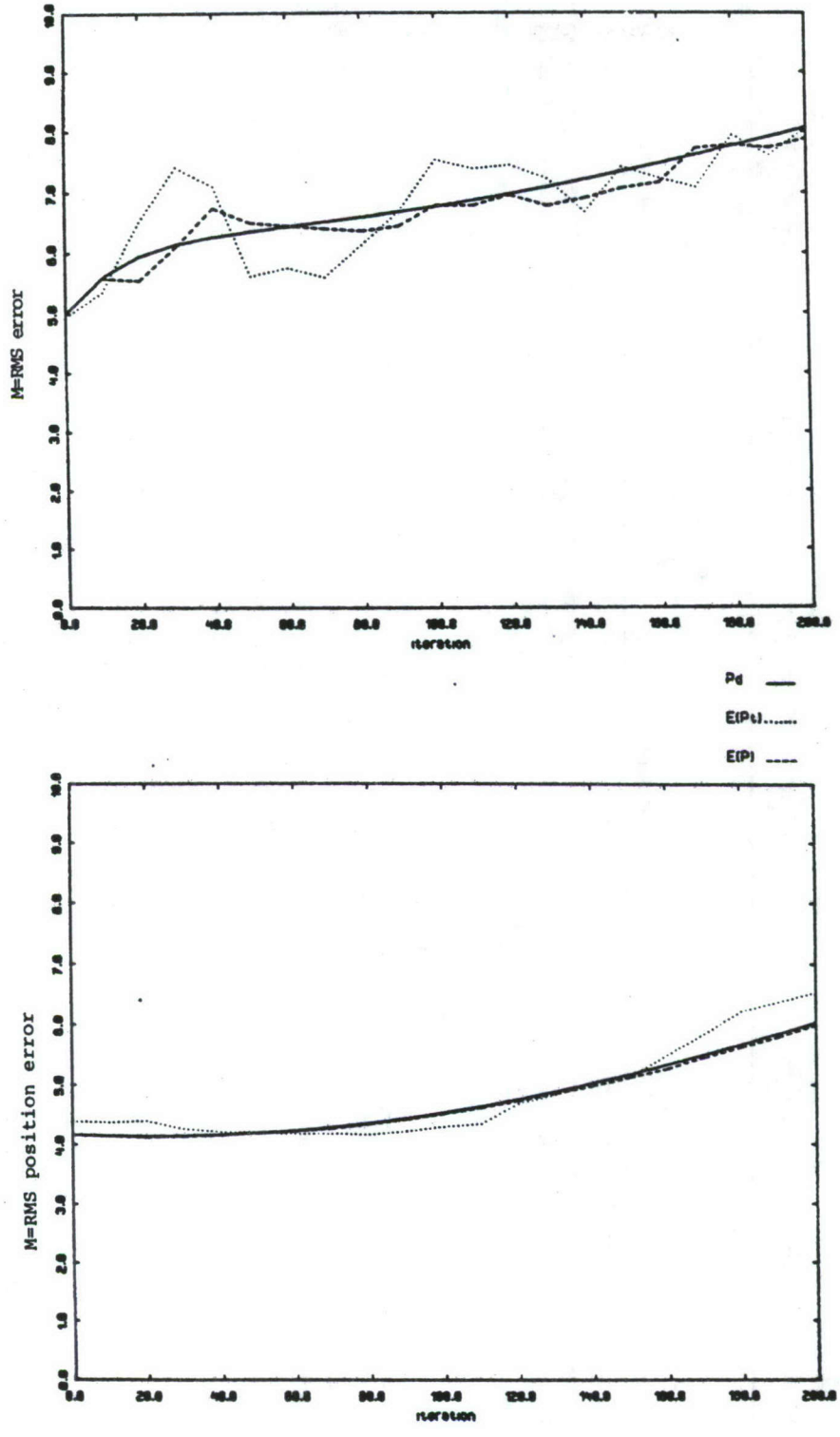

Figure 17. $M \cdot \underline{P}^{d}_{k|k}$, $M \cdot E\{\underline{P}^{t}_{k|k}\}$, and $M \cdot E\{\underline{P}_{k|k}\}$ for $(P_D, P_F) = (.4, .06)$

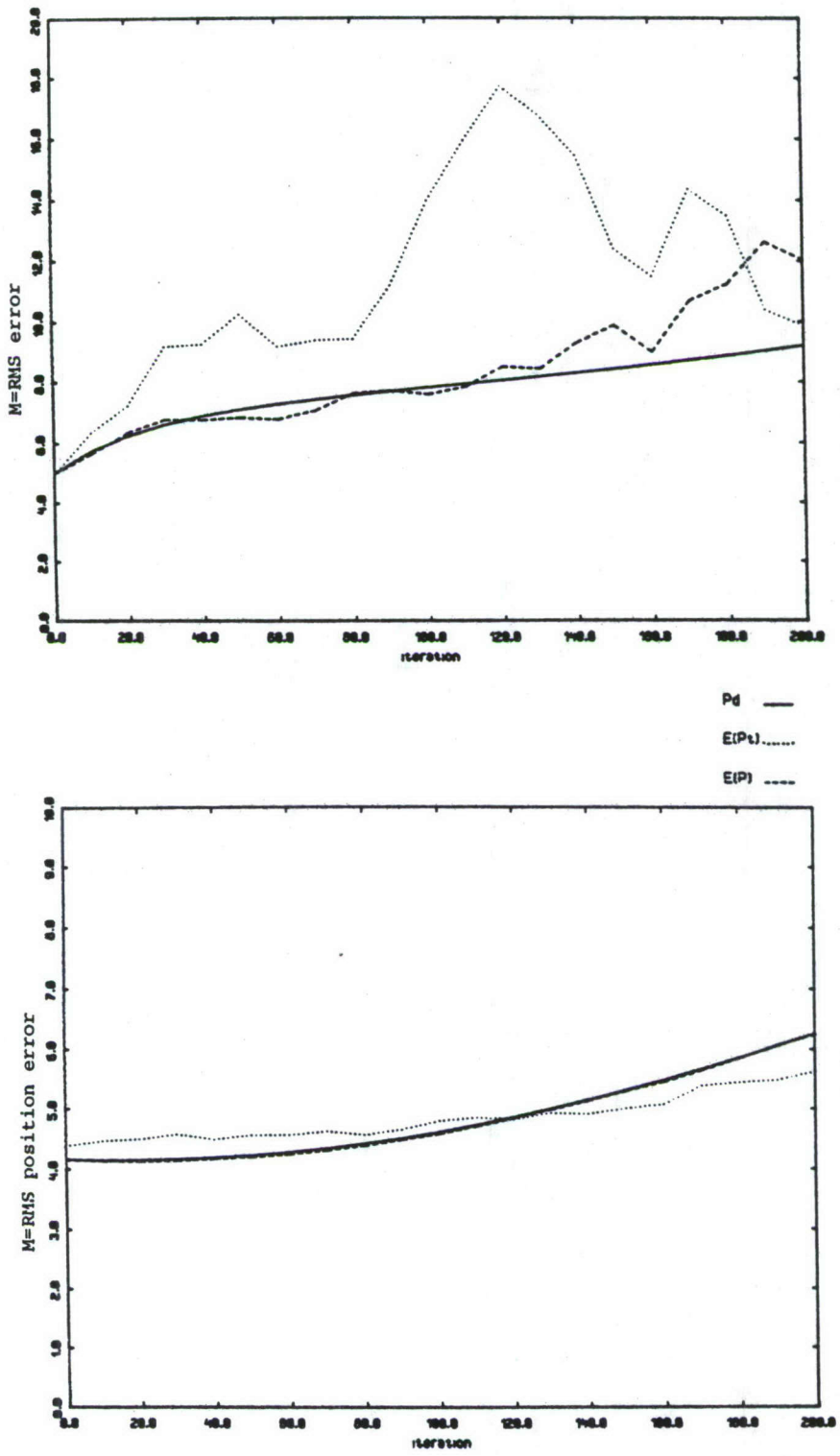

Figure 18. $M \cdot \underline{P}^{d}_{k|k}$, $M \cdot E\{\underline{P}^{t}_{k|k}\}$, and $M \cdot E\{\underline{P}_{k|k}\}$ for $(P_D, P_F) = (.3, .07)$ (note that scale of RMS error is different from other figures)

REFERENCES

1. R. E. Kalman and R. S. Bucy, "New Results in Filtering and Prediction Theory," Trans. ASME: J. Basic Eng., Vol. 83, March 1961, pp. 95-108.

2. I. B. Rhodes, "A Tutorial Introduction to Estimation and Filtering," IEEE Trans. Auto. Control, Vol. AC-16, December 1971, pp. 688-706.

3. A. H. Jazwinski, Stochastic Processes and Filtering Theory, Academic Press, 1970.

4. P. S. Maybeck, Stochastic Models, Estimation, and Control -- Volume 1, Academic Press, 1979.

5. B. D. O. Anderson, Optimal Filtering, Prentice-Hall, 1979.

6. Y. Bar-Shalom and E. Tse, "Tracking in a Cluttered Environment with Probabilistic Data Association," Automatica, Vol. 11, September 1975, pp. 451-460.

7. T. E. Fortmann and S. Baron, "Problems in Multi-Target Sonar Tracking," Proc. 1978 IEEE Conf. on Decision and Control, San Diego, California, January 1979.

8. T. E. Fortmann, Y. Bar-Shalom, and M. Scheffé, "Sonar Tracking of Multiple Targets Using Joint Probabilistic Data Association," IEEE Journal of Oceanic Engineering, Vol. OE-8, July 1983, pp.173-184 (also appeared in Proc. 1980 IEEE Conf. on Decision and Control, Albuquerque, New Mexico, December 1980).

9. R. Singer, R. Sea, and K. Housewright, "Derivation and Evaluation of Improved Tracking Filters for use in Dense Multitarget Environments," IEEE Trans. Info. Theory, Vol. IT-20, July 1974, pp. 423-432.

10. D. B. Reid, "An Algorithm for Tracking Multiple Targets," IEEE Trans. Auto. Control, Vol. AC-24, December 1979, pp. 843-854.

11. E. Taenzer, "Tracking Multiple Targets Simultaneously with a Phased Array Radar," IEEE Trans. Aerospace and Electronic Systems, Vol. AES-16, September 1980, pp. 604-614.

12. C. L. Morefield, "Application of Ø-1 Integer Programming to Multitarget Tracking Problems," IEEE Trans. Auto. Control, Vol. AC-22, June 1977, pp. 3Ø2-312.

13. D. L. Alspach, "A Gaussian Sum Approximation to the Multitarget Identification - Tracking Problem," Automatica, Vol. 11, May 1975, pp. 285-296.

14. R. W. Sittler, "An Optimal Data Association Problem in Surveillance Theory," IEEE Trans. Mil. Electron., Vol. MIL-8, April 1964, pp. 125-139.

15. Y. Bar-Shalom, "Tracking Methods in a Multi-Target Environment," IEEE Trans. Auto. Control, Vol. AC-23, August 1978, pp. 618-626.

16. H. L. Wiener, W. W. Willman, I. R. Goodman, and J. H. Kullback, "Naval Ocean-Surveillance Correlation Handbook, 1978," NRL Report 834Ø, Naval Research Lab, October 1979.

17. I. R. Goodman, H. L. Wiener, and W. W. Willman, "Naval Ocean-Surveillance Correlation Handbook, 1979," NRL Report 84Ø2, Naval Research Laboratory, September 198Ø.

I8. T. E. Fortmann and Y. Bar-Shalom, "Modification of the Likelihood Function to Account for Probabilistic Data Association," BBN Report 3964A (revised), Bolt Beranek and Newman Inc., November 1979, Contract NØØØ39-78-C-Ø296.

19. A. D. Whalen, Detection of Signals in Noise, Academic Press, 1971.

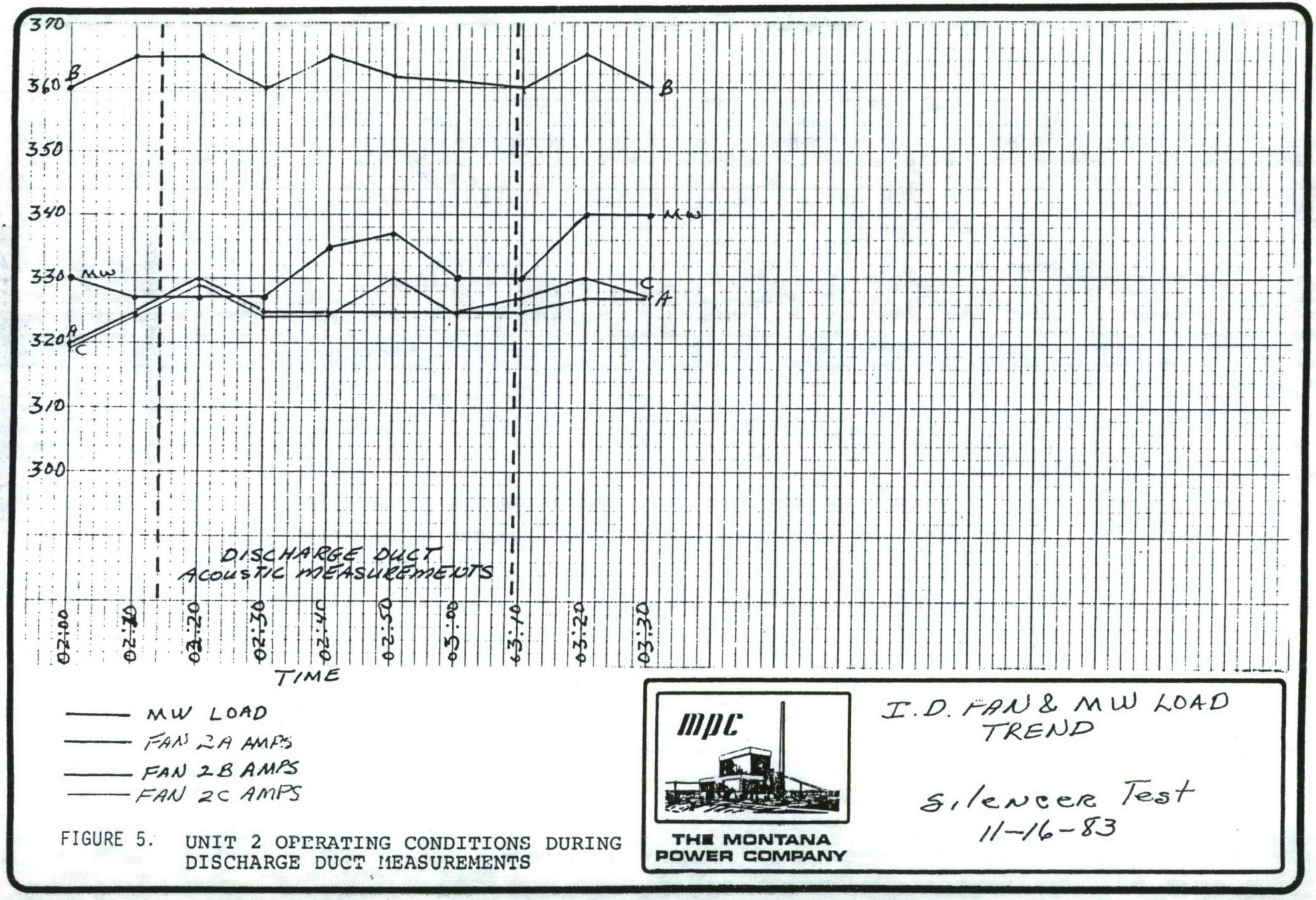

FIGURE 5. UNIT 2 OPERATING CONDITIONS DURING DISCHARGE DUCT MEASUREMENTS

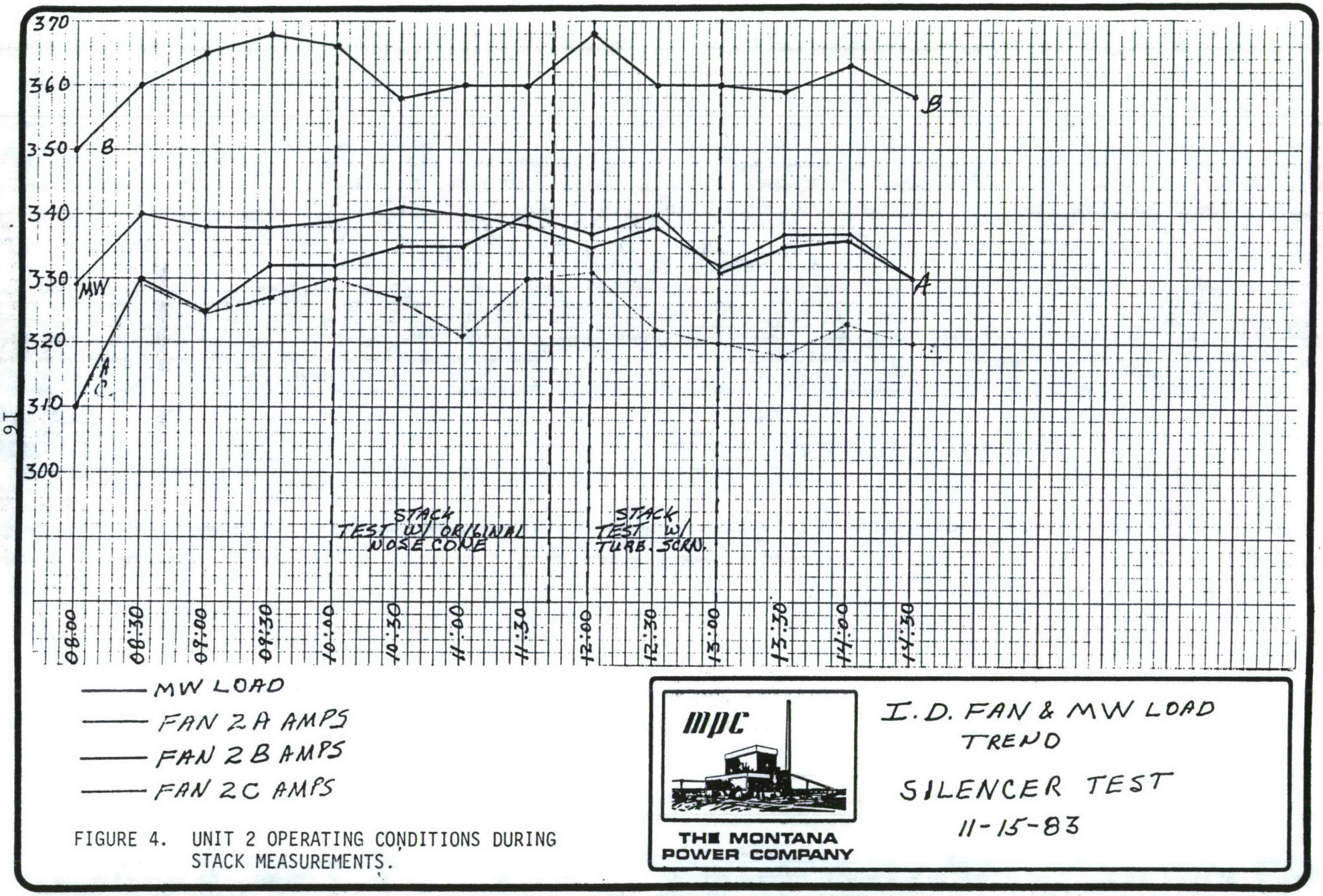

FIGURE 4. UNIT 2 OPERATING CONDITIONS DURING STACK MEASUREMENTS.

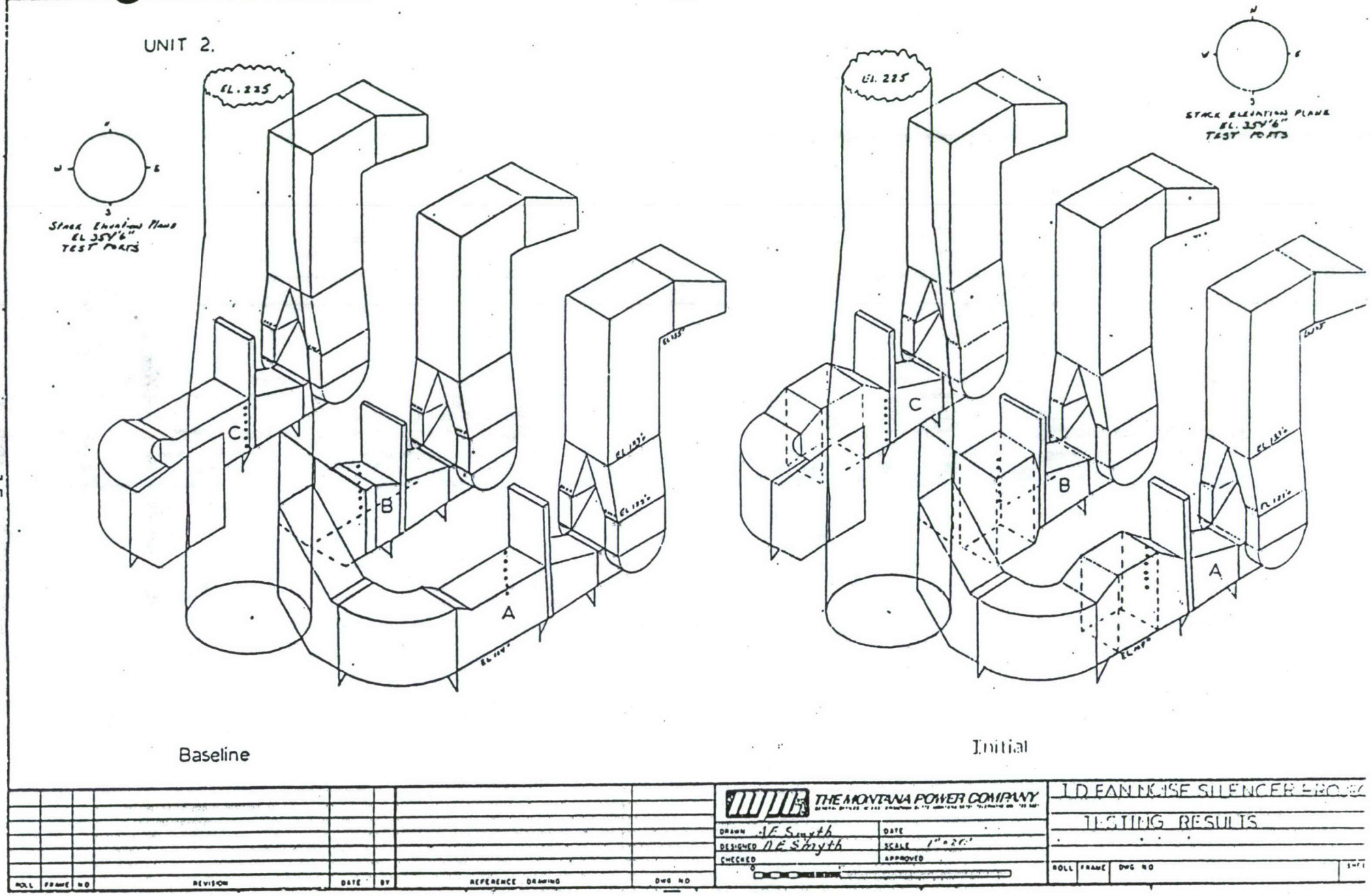

FIGURE 3. SKETCH OF COLSTRIP UNIT 2 ID FANS, DUCTS, AND STACK SHOWING MEASUREMENT LOCATIONS.

FIGURE 2. GENERAL ARRANGEMENT OF COLSTRIP UNIT 1 GAS PATH FROM SCRUBBER OUTLET TO STACK. UNIT 2 ARRANGEMENT IS MIRROR IMAGE.

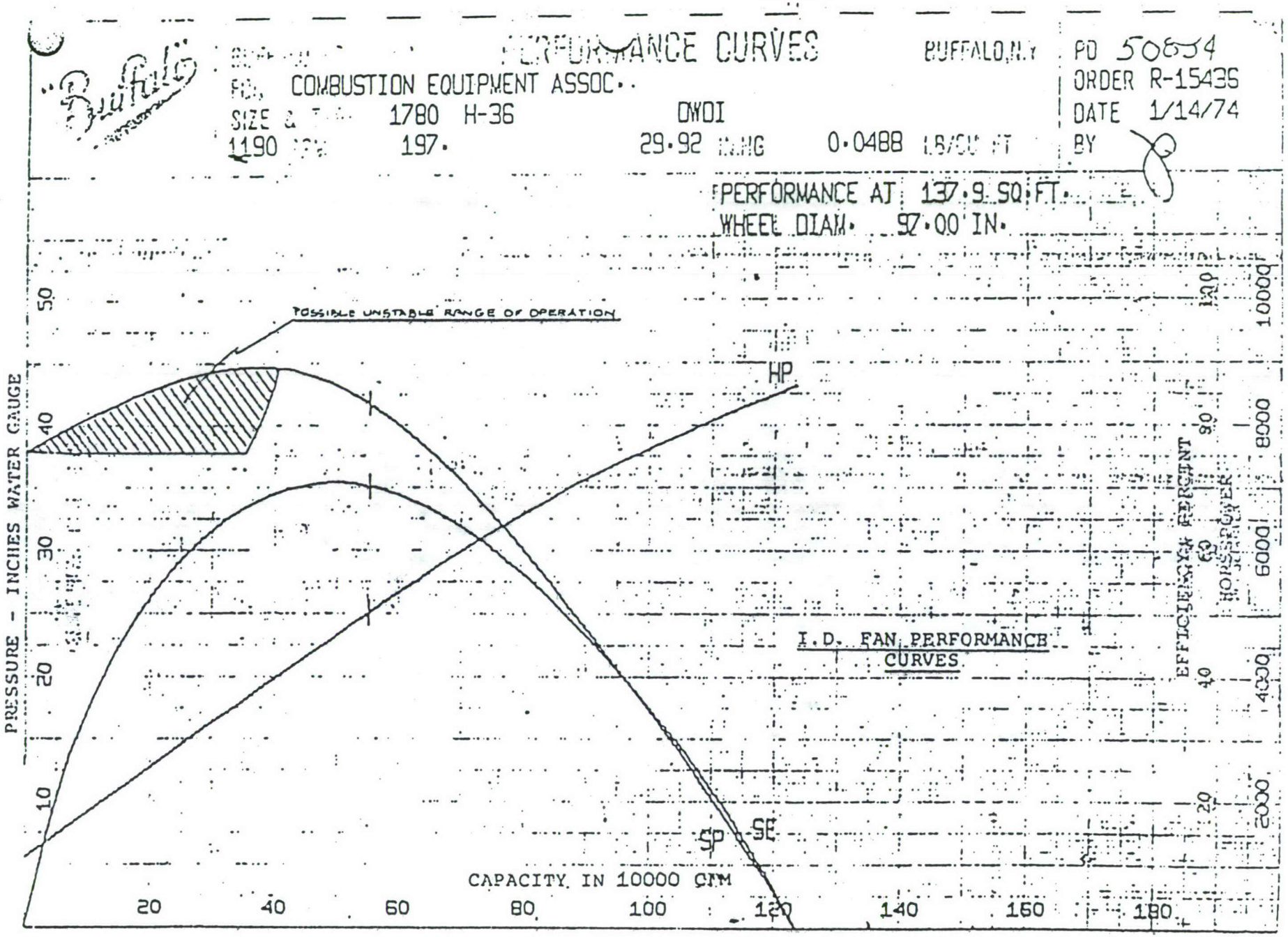

FIGURE 1. FAN MANUFACTURERS PERFORMANCE CURVES FOR COLSTRIP UNIT 1 AND 2 ID FANS OPERATING AT SPECIFIED GAS CONDITIONS.